A geometric optics method for high frequency electromagnetic fields computations near fold caustics - Part II - The energy

Jean-David Benamou, Olivier Lafitte, Rémi Sentis, Ian Solliec

INRIA

INSTITUT NATIONAL DE RECHERCHE EN INFORMATIQUE ET EN AUTOMATIQUE

A geometric optics method for high frequency electromagnetic fields computations near fold caustics - Part II - The energy

J.-D. Benamou, O. Lafitte, R. Sentis and I. Solliec

N° 4627

novembre 2002

THÈME 4

ISSN 0249-6399 ISRN INRIA/RR--4627--FR+ENG

INRIA
ROCQUENCOURT

A geometric optics method for high frequency electromagnetic fields computations near fold caustics - Part II - The energy

J.-D. Benamou, O. Lafitte, R. Sentis and I. Solliec

Thème 4 — Simulation et optimisation
de systèmes complexes
Projet OTTO

Rapport de recherche n° 4627 — novembre 2002 — 62 pages

Abstract: This paper is a sequel of [3] and presents the computation of the amplitudes needed to evaluate the energy deposited by the laser wave in a plasma when a fold caustic forms.

Key-words: Hamilton-Jacobi, Hamiltonian System, Ray Tracing, Viscosity Solution, Upwind Scheme, Geometric Optics, Eave Equation, Laser, Plasma, Electromagnetism, Laser Méga-Joule

Unité de recherche INRIA Rocquencourt
Domaine de Voluceau, Rocquencourt, BP 105, 78153 Le Chesnay Cedex (France)
Téléphone : +33 1 39 63 55 11 — Télécopie : +33 1 39 63 53 30

Une méthode de calcul de champs electromagnétiques hautes fréquences au voisinnage de caustiques de type pli basée sur l'optique géométrique - Deuxième partie - L'énergie

Résumé : Ce papier, la suite de [3], présente le calcul des amplitudes nécessaire pour évaluer l'énergie déposée par une onde laser dans un plasma en présence d'une caustique de type pli.

Mots-clés : Hamilton-Jacobi, Système Hamiltonien, Lancer de rayons, Solution de Viscosté, Schéma Décentrés, Optique Géométrique, Equation des Ondes, Laser, Plasma, Electromagnétisme, Laser Méga-Joule

1 Introduction

This paper is the second and last part (the first part is [3]) presenting a Eulerian numerical method for the simulation of the propagation of a laser wave in a material medium.

The electromagnetic field A is the solution of the following frequency wave equation (see [8])

$$\nabla \cdot (\nabla A) + k_0^2 n^2 A + i\nu k_0 A = 0. \tag{1}$$

The space variable X belongs to $\mathbf{R}^{d+1}$ ($d = 1$ in the sequel), ∇ is the gradient operator in $\mathbf{R}^{d+1}$, k_0 is the wave number of the laser wave in the vacuum, $n = n(X)$ is a given smooth positive function which corresponds to the refractive index of the medium and ν a positive parameter characterizing the absorption coefficient of the laser energy by the material. The system is subject to an incident plane wave

$$A_{inc} = A_0 \exp(ik_0 X.(\cos\alpha, \sin\alpha)) \tag{2}$$

where α is the angle of incidence and the scattered field $A_{scat} = A - A_{inc}$ satisfies radiation boundary conditions at infinity.

As in [3], a WKB technique is used (see for example [7]). In its simplest form the oscillatory unknown A is approximated by

$$A \simeq a e^{ik_0\phi}. \tag{3}$$

An asymptotic expansion of equation (1) shows that the phase ϕ is solving the eikonal equation

$$|\nabla\phi|^2 = n^2 \tag{4}$$

and the amplitude a is a solution to

$$\nu a + 2\nabla a \nabla\phi + a\nabla.(\nabla\phi) = 0. \tag{5}$$

The physical quantity $E = |a|^2$ which represents the laser energy satisfies

$$\nu E + \nabla.(E\nabla\phi) = 0 \tag{6}$$

Both geometrical optics unknowns ϕ and a have slow variations compared to A and are cheaper to approximate and compute in terms of computational cost. The WKB approximation is often the only affordable way to simulate high frequency wave propagation phenomena.

It is however well known that the single phase ansatz (3) is not correct in the vicinity of caustics for two related reasons: first, the rays which are the integral curves of the gradient

of the phase $\nabla\phi$ and along which ϕ is defined cross and define a multi-valued phase function. Second the same rays are the characteristics of the conservation law (6). Near the caustic neighboring rays cross and the laplacian of the phase $\nabla.(\nabla\phi)$ is singular at the caustic. Eventually, the energy E computed by means of the WKB approximation becomes infinite.

The appropriate generalization of (3) is the Maslov theory of global oscillatory functions, which can be presented along the lines of the theory of Fourier Integral Operators of Hörmander ([6]). As an introduction, we treat a most simple example (already used in [3]) and show how the solution of (1) is linked to the notion of multi-valued solution of (4-5) : Let us consider a 2-D half space problem $\{X = (x, z) \in bfR^2 \mid x > 0\}$ which will simplify into a 1-D problem as we assume the medium to be characterized by a simple index $n^2(z, x) = 1 - x$. The incoming wave determines the boundary condition data at $x = 0$, and since n does not depend on z we can seek a solution of the form $A(z, x) = u(x)\exp(iz\sin\alpha)$. Equation (1) then simplifies to

$$u''(x) + k_0^2(x_c - x)u(x) + ik_0\nu u = 0$$

where $x_c = \cos^2\alpha$.

The only "physical" solution (compatible with the radiation boundary condition) is :

$$u(x) = Ck_0^{1/6}\mathrm{Ai}\left(-k_0^{2/3}((x_c - x) + i\nu k_0^{-1})\right)$$

the coefficient $k_0^{1/6}$ standing here for normalization purposes. For $x < x_c$, as $k_0 \to +\infty$, we show, using the classical asymptotic expansion of the Airy function (see annex 7.1), that

$$u(x) \simeq \frac{C}{2\sqrt{\pi}}\left(\frac{e^{-i\pi/4}}{(x_c - x)^{1/4}}\exp(ik_0\zeta) + \frac{e^{+i\pi/4}}{(x_c - x)^{1/4}}\exp(-ik_0\zeta)\right) + O(k_0^{-1})$$

where

$$\zeta = \frac{2}{3}(x_c - x + i\nu k_0^{-1})^{3/2}$$

that is to say

$$u(x) \quad \simeq \quad a^+e^{-i\pi/4}\exp(ik_0\xi) \quad + \quad a^-e^{+i\pi/4}\exp(-ik_0\xi) \quad + \quad O(k_0^{-1}) \quad (7)$$

where $\xi = \frac{2}{3}(x_c - x)^{3/2}$ and

$$a^- = \frac{C}{2\sqrt{\pi}}\frac{1}{(x_c - x)^{1/4}}e^{\nu\sqrt{x_c - x}}, \quad a^+ = \frac{C}{2\sqrt{\pi}}\frac{1}{(x_c - x)^{1/4}}e^{-\nu\sqrt{x_c - x}} \quad (8)$$

We can easily identify (7) as the sum of two W.K.B ansatz formed by the $\pm$ branches. Indeed, as in [3], we can see that the rays of geometrical optics for this simplified toy problem produce a fold straight caustic curve $x = x_c$ (see figure 1). Each point on the illuminated side of the caustic is reached by two rays which are labeled $-$ and $+$. The $-$ part of the rays propagate

unto the caustic and is called direct while the + part is the return portion of the rays after passing the caustic. These two families define two phases

$$\phi^{\pm} = z\sin\alpha \pm \frac{2}{3}(x_c - x)^{3/2} + C \tag{9}$$

which are solution of (4) with ad-hoc initial and boundary conditions (the constant C depends on the boundary condition). Then we get the following approximation for the potential $A = u\exp(iz\sin\alpha)$:

$$A \simeq a^- e^{-i\pi/4}\exp(ik_0\phi^-) + a^+ e^{i\pi/4}\exp(ik_0\phi^+) + O(k_0^{-1}). \tag{10}$$

Formula (10) means that at high frequency, A is the sum of two W.K.B ansatz formed by the $\pm$ branches. The $e^{\pm i\pi/4}$ terms represent the known $\frac{\pi}{2}$ phase shift across caustics according to Maslov theory. On figure 2, we have plotted in the case $\nu = 0$ both the exact solution A (plain line) and its W.K.B. approximation (stars) (only in the last wavelength is a difference to be seen, the approximation blows at the caustic). A valid approximation of A near the caustic in the spirit of [11] is proposed in [9]).

From the application point of view the important physical quantity is the absorbed laser energy $\int_D \nu|A|^2 dX$ on a fixed domain D. One can readily check from (7)

$$|A|^2 \simeq (|a^+|^2 + |a^-|^2) + -2a^+a^- sin(2k_0\zeta) + O(k_0^{-1})$$

Recall that this approximation holds asymptotically in k_0 and therefore only the stationary points of ζ will contribute to the integral of the last term, actually only the caustic point. When the domain D is a strip $[x_1, x_2]$ which does not contain the caustic, we get by the stationary phase formula

$$\int_{x_1,x_2} |A|^2 dx = \int_{x_1,x_2} (|a^+|^2 + |a^-|^2)dx + O(k_0^{-\frac{1}{3}}) \tag{11}$$

In appendix A, we actually prove in the affine index of refraction case that (11) holds even if x_2 is at the caustic point x_c .

The numerical method presented in [3] and in this paper is designed to work for index of refraction $n(z,x)$ producing a fold caustic that can be parameterized by z, i.e. the caustic is represented by the curve $x = x_c(z)$. One can check (see [9] for a detailed demonstration of this result) that, when $\nu = 0$, formula (10) still holds away from the caustic.

In general cases, the phases $\phi^{\pm}$ and the amplitudes $a^{\pm}$ can only be computed numerically, the classical method being ray tracing. In [3], we proposed an Eulerian method for the computation of $\phi^{\pm}$. In this paper, we focus on the specific difficulties linked to the computation of the amplitudes and in particular the square of the amplitudes $E^{\pm} = |a^{\pm}|^2$. Because of the singularity of the phase coefficients at the caustic neither (5) for $a^{\pm}$ nor (6)

for $E^{\pm}$ are used in practice. Instead we use the conservative properties of equation (6) to establish the following representation for the energies

$$E^{\pm} = \frac{Z^{\pm}}{|\Theta^{\pm}|\partial_z \phi^{\pm}} \tag{12}$$

where Θ is the oriented volume of an infinitesimal tube of rays (sometimes called "geometrical spreading") which vanishes at the caustic and Z is a function decaying along the rays at a rate governed by ν. These new unknowns are solutions of Eulerian transport equations and provide a robust evaluation of across caustics.

The paper is organized as follows. We first summarize basic facts and results from [3] on the bi-valued phase $\phi^{\pm}$. We then derive in section 3 the equations we will use to compute the amplitudes and numerically evaluate formula (11). Section 4 details more technical results on the modification of the computational domain and boundary/initial conditions. Section 5 explains the difficulty linked to the finite difference approximation of the transport equation near the caustic. We propose a first order scheme and show numerical results. Finally section 6 shows numerical results and presents a numerical validation of formula (10) and (11) in the 1-D case.

2 From the Lagrangian to the Eulerian modelization of the fold caustic

We give in the two following subsection, a necessary overview of the phase model presented in [3]. This presentation is slightly different and hopefully clearer than the one that can be found in [3].

In this section and throughout the paper we use $d = 1$ that is $X = (z, x)$ is in R^2 and $\nabla = (\partial_z, \partial_x)$. We believe that the content of this paper can be extended to treat fold caustic cases in three dimensions ($d = 2$ and ∂_x is a gradient).

2.1 The Lagrangian model of the geometric optics

We start with an infinite device because it is in essence what our proposed Eulerian method can handle. The index $n(z, x)$ is constant ($= 1$) in the half plane $x < 0$ where the incident plane wave (2) propagates freely. The important assumption on the physics of the problem in [3] - still valid in this paper - was an a priori hypothesis on a qualitative behavior of the rays. In our (x, z) setting (see figure 4), we use the z axis as a privileged direction of propagation. The rays start as straight lines making an angle α with the vertical axis in the $x < 0$ half plane (constant index of refraction), then they enter the $x > 0$ area where the index has smooth variations such that rays "folds" and the locus of the fold is called the caustic. After turning back at the caustic the rays eventually exit the $x > 0$ domain and

revert to a straight line in the constant index part of the medium.

The "fold caustic" assumption can be mathematically expressed by two conditions. First the ray curves can be parameterized by z and so is the caustic denoted by $x = x_c(z)$. Second, every point (x, z) on the illuminated side of the caustic is passed by two rays, the other side (the shadow zone) is not reached. They can be classified into two "branches" : *direct* rays that reach the point before passing through the caustic and *return* rays that reach the point after.

We define the family of ray curves $\{y(z, z_0),\ z_0 \in \mathbf{R},\ z > z_0\}$ (see figure 4) where z_0 indicates the first crossing position of the ray with the $x = 0$ axis (Γ_{inc}). The rays are solutions, $\forall z_0$ and $\forall z > z_0$ of the 1-D Hamiltonian system :

$$\begin{cases} \dot{y}(z, z_0) = H_p(z, y, p) \\ \dot{p}(z, z_0) = -H_x(z, y, p) \\ \dot{\varphi}(z, z_0) = p \cdot H_p(z, y, p) - H(z, y, p) \end{cases} \tag{13}$$

where $H(z, x, p) = -\sqrt{n^2 - p^2}$. The dot stands for derivation with respect to z, and H_x and H_p denote the derivatives of H with respect to x and p. We specify the initial conditions on the axis $x = 0$

$$\begin{cases} y(z_0, z_0) = 0 \\ p(z_0, z_0) = \sin\alpha \\ \varphi(z_0, z_0) = \sin\alpha\, z_0 \end{cases} \tag{14}$$

The initial conditions are derived from the incident plane wave condition (2) and all rays can be extended backwards by straight lines (they solve the same equation in the $x < 0$ zone).

2.2 The truncated and extended Lagrangian model

The truncated Lagrangian model

In practice our device is finite and the index n defined in a bounded interval. We can still assume the domain to be infinite in the $x < 0$ half plane as the propagation is trivial there but we need also to bound the domain in the z direction. Let us set $]0, Z[$ as the range in z where the index is defined. There is no difficulties to stop the ray computations at $z = Z$ and truncate the domain there. Truncating at $z = 0$ is more problematic. Notice indeed that is we use the same initialization (14) but only for positive z_0. It generates different zones where the fold caustic hypothesis above does not necessarily applies. There is a first zone labeled (1) on figure 5 below the first ray shot from the origin $(0, 0)$, represented in thick line, which is not covered by any rays. A second zone labeled (2) delimited by the direct part and return part of that same first ray is only reached by direct rays. We finally on the remaining part of the illuminated domain, labeled (3) on the figure where we get the usual "fold caustic" regime where every point is reached by a direct and a return ray.

The extended Lagrangian model

As already hinted, and extensively explained in [3], the truncation of the Lagrangian model is a source of difficulties where its Eulerian treatment is concerned. Indeed, both the direct and return part of the solution are sought for as coupled Eulerian solutions of evolution partial differential equations in z and the coupling cannot be avoided to compute the caustic. Initial conditions are therefore needed for both branches at $z = 0$.

In [3] we proposed initial conditions derived from a compatible stationary problem : the index is first extended in the $z < 0$ by setting $n(z, x) = n(0, x),\ \forall z < 0$. As the z dependence is suppressed, all rays issued from negative z_0 have the same behavior and the caustic is a straight line $x_c(z) = C_0$. It can be shown [10] that this stationary solution and our physical solution connect smoothly without interference (see figure 6). This extension process has two advantages. First we now have two branches everywhere in the physical domain, second the stationary solutions at $z = 0$ are easy to compute and can be used as initial data.

We can therefore truncate anew this extended model at $z = 0$ and set the initial conditions for the ray system on the x axis (figure 7). Note that according to the "fold caustic" hypothesis each point $(z = 0, x_0)$ for $x_0 \in]-\infty, C_0[$ is reached by two rays of the extended model. We now have two families of rays curves $\{y_i(z, x_0),\ x_0 \in]-\infty, C_0[,\ z > 0\}$ for $i = 1, 2$ where $y_1(z, x_0)$, respectively $y_2(z, x_0)$, are the rays issued from the direct, respectively return, rays crossing $z = 0$ at x_0. The rays of each family satisfy for $\forall z > 0$ of the same system (13) and the initial conditions now derive from truncating the extended model :

$$\begin{cases} y_i(0, x_0) = x_0 \\ p_i(0, x_0) = p_{i,0}(x_0) \\ \varphi_i(0, x_0) = \varphi_{i,0}(x_0) \end{cases} \tag{15}$$

where $p_{1,0}$ and $\varphi_{1,0}$ are data of the problem, $p_{2,0}$ and $\varphi_{2,0}$ are by-products of the stationary problem in $z < 0$ and $p_i(., x_0)$ and $\varphi_i(., x_0)$ are the corresponding solutions of (13).

2.3 From Lagrangian to Eulerian

The rays of the y_2 family will always be return rays, they passed the caustic in the extension $x < 0$ of the domain ; we will denote these rays y_2^+. This is not the case for the y_1 family in which the rays start as direct rays, pass the caustic and become return rays (figure 3). The direct part of a y_1 rays will be denoted y_1^- and the return part y_1^+. Mathematically, $\forall x_0$, there is a depth $z_c(x_0)$ such that

$$y_1(z_c(x_0), x_0) = x_c(z_c(x_0))$$

and then

$$\begin{aligned} y_1^-(z, x_0) &= y_1(z, x_0),\ for\ z \leq z_c(x_0) \\ y_1^+(z, x_0) &= y_1(z, x_0),\ for\ z \leq z_c(x_0). \end{aligned}$$

We can now assert that every point $(z,x) \in]0,Z[\times]0,x_c(z)[$ is passed by two rays (figure 1) : a direct ray which is necessarily a y_1^- rays and a return ray which is either a y_1^+ or a y_2^+ ray. Thus, for all x_0 the formulae

$$\phi^-(z, y_1^-(z,x_0)) = \varphi_1(z,x_0). \tag{16}$$

for the direct branch and

$$\phi^+(z, y_1^+(z,x_0)) = \varphi_1(z,x_0), \quad \phi^+(z, y_2^+(z,x_0)) = \varphi_2(z,x_0) \tag{17}$$

for the return branch, define two single valued Eulerian phase functions $\phi^+(z,x)$ and $\phi^-(z,x)$.

We recall the full Eulerian model for $\phi^\pm$ and associated initial and boundary conditions derived in [3]

$$\partial_z \phi^\pm(z,x) + H(z,x,\nabla_x \phi^\pm) = 0 \text{ for } (z,x) \in R^+ \times [0, x_c(z)] \tag{18}$$

We use an incoming boundary conditions on ϕ^-

$$\phi^-(z,0) = \phi_{inc}(z) \text{ for } z \geq 0. \tag{19}$$

Initial conditions are derived from a compatible stationary problem [3] (we return to this in section 4.1).

The direct and return phases (and, as they satisfy the same equation, their gradient) match at the caustic

$$\phi^+(z, x_c(z)) = \phi^-(z, x_c(z)) \text{ for } z \geq 0. \tag{20}$$

and one can check that

$$\dot{x}_c(z) = H_p(z, x_c(z), p_c(z)), \qquad p_c(z) = \partial_x \phi^\pm(z, x_c(z)) \tag{21}$$

Both (21) and (18) are consequences of the identification formula

$$p(z,x_0) = \partial_x \phi(z, y(z,x_0)) \tag{22}$$

which holds for both families of rays or branches. We use this property to define the Eulerian flows :

$$\mathcal{V}^\pm(z,x) = H_p(z,x,\partial_x \phi^\pm(z,x)) = -\frac{\partial_x \phi^\pm(z,x)}{H(z,x,\partial_x \phi^\pm(z,x))} = -\frac{\partial_x \phi^\pm(z,x)}{\partial_z \phi^\pm(z,x)}$$

corresponding to the Lagrangian flows, i.e. the first line of (13).

Eulerian-Lagrangian function correspondence

As already done for the bi-valued phase (16-17), we systematically define bi-valued Eulerian function from their Lagrangian counterparts. We consider a couple of Lagrangian functions $\mathbf{U}_1(z,x_0)$ and $\mathbf{U}_2(z,x_0)$ which are transported along the $y_{1,2}$ rays according to the ordinary differential equation

$$\partial_z \mathbf{U}_i = f(\mathbf{U}_i),$$

As in (16-17) , we again define two Eulerian functions $U^{\pm}(z,x)$ by

$$U^-(z,y_1^-(z,x_0)) = \mathbf{U}_1(z,x_0), \quad U^+(z,y_i^+(z,x_0)) = \mathbf{U}_i(z,x_0)\ i=1,2,\ \forall x_0. \tag{23}$$

Remark : As rays y_1^+ and y_2^+ never cross we will in the sequel unambiguously note simply y^+ for the return rays and y^- for the direct rays (instead of y_1^-).

The Eulerian functions satisfy the partial differential equations obtained by deriving the above relations

$$\partial_z U^{\pm} + \mathcal{V}^{\pm}(z,x)\cdot\partial_x U^{\pm} = f(U^{\pm}(z,x))$$

that is to say

$$\partial_z\phi^{\pm}\partial_z U^{\pm} + \partial_x\phi^{\pm}\cdot\partial_x U^{\pm} = \partial_z\phi^{\pm} f(U^{\pm}(z,x)) \tag{24}$$

Remark also that branches necessarily match at the caustic

$$U^+(z,x_c(z)) = U^-(z,x_c(z)) \tag{25}$$

We already used this expression for the phases (20) and will use it again to derive boundary conditions.

3 The energy/amplitude model

The aim of this subsection is explain how the energies $E^{\pm} = |a^{\pm}|^2$ used in the conjectured formula (11) are evaluated. The classical method for the computation of the energy uses a Lagrangian formula obtained from the integration of (6) on a ray tube. We first detail this derivation leading to formula (12) and introduce geometrical spreading $\Theta^{\pm}$ and the auxiliary variables $Z^{\pm}$. We then give the Eulerian equations used to compute these new quantities. Finally we give an equivalent fully Eulerian derivation of the same equations.

3.1 The Lagrangian approach for $E\pm$

We start by considering a tube around a reference ray $y^-(z,\bar{x}_0)$ in the direct part of the Lagrangian solution and will omit the $.^-$ notation for convenience. A ray tube is defined as $\Omega = \{(z,y(z,x_0)),\ z\in]z_0,z_1[,\ x_0\in B(\bar{x}_0,\epsilon)\}$ where $B(\bar{x}_0,\epsilon)$ is the ball of radius ϵ and

center $\bar{x}_0$, and z_0, z_1 are fixed (see figure 8). The integration of equation (6) on Ω gives (by Green's formula)

$$\int_{\{z=z_1\}\cap\partial\Omega} E(z_1,x)\nabla\phi(z_1,x)\cdot\vec{n}\,dx = \int_{\{z=z_0\}\cap\partial\Omega} E(z_0,x)\nabla\phi(z_0,x)\cdot\vec{n}\,dx + \int_\Omega \nu E(z,x)\,dxdz$$

where $\vec{n}$ is the exterior normal to $\partial\Omega$. It is simply here $(\pm 1, 0)$ in the two terms above and then $\nabla\phi\cdot\vec{n} = \pm\partial_z\phi$. The remaining parts of $\partial\Omega$ are rays portions and their contribution is zero as $\nabla\phi$ is tangent to the rays by construction.

We now change the integration variable $x \to x_0 = y^{-1}(z,x)$ (i.e. $x = y(z,x_0)$) :

$$\int_{B(\bar{x}_0,\epsilon)} E(z_1,y(z_1,x_0))\partial_z\phi(z_1,y(z_1,x_0))|\partial_{x_0}y(z_1,x_0)|\,dx_0 = \int_{B(\bar{x}_0,\epsilon)} E(z_0,y(z_0,x_0))\partial_z\phi(z_0,x_0)\,dx_0 + \int_{z_0}^{z_1}\int_{B(\bar{x}_0,\epsilon)} \nu E(z,y(z,x_0))|\partial_{x_0}y(z,x_0)|\,dx_0dz$$

and obtain a formula for the energy - along every ray ($\forall x_0$) and for all $z \in]z_0, z_1[$ - by letting ϵ go to 0

$$E(z,y(z,x_0))\partial_z\phi(z,y(z,x_0))|\partial_{x_0}y(z,x_0)| = E(z_0,x_0)\partial_z\phi(z_0,x_0)|\partial_{x_0}y(z_0,x_0)| + \int_{z_0}^{z}\nu E(z,y(z,x_0))|\partial_{x_0}y(z_0,x_0)|\,dz. \quad (26)$$

Let us assume for a while that $\nu = 0$. Then equation (26) simply states the well-known conservation property according to which $E\times(\partial_z\phi\cdot|\partial_{x_0}y|)$ is constant along rays. Indeed the oriented volume of an infinitesimal tube of rays reduces to $\partial_z\phi|\partial_{x_0}y|$ in the paraxial model.

Of course, formula (26) is meaningful as long as the ray tube does not collapse ; we recall that we are in the direct part of the rays and $\partial_{x_0}y^-(z,x_0) \neq 0$. At caustic points, $\partial_{x_0}y^-(z,x_0)$ vanishes and (26) predicts and infinite energy. To overcome the caustic difficulty we define a new function $Z^-(z,x)$:

$$Z^-(z,y^-(z,x_0)) = E(z,y^-(z,x_0))\partial_z\phi^-(z,y^-(z,x_0))|\partial_{x_0}y^-(z,x_0)|. \quad (27)$$

We find from (26) that $Z^-(z,y^-(z,x_0))$ satisfies the ODE

$$\begin{aligned}\partial_z\{Z^-(z,y^-(z,x_0))\} &= -\nu\frac{Z^-(z,y^-(z,x_0))}{\partial_z\phi^-(z,y^-(z,x_0))}\\ Z^-(0,x_0) &= E(0,x_0)\partial_z\phi^-(0,x_0)\end{aligned} \quad (28)$$

(recall that $y(0,x_0)=x_0$). Thus, as we assumed $\partial_z\phi>0$ (section 2.1), Z^- remains bounded even at the caustic.

We now can repeat the above computations in the return part of the solution and in particular a Z^+ function can be defined that satisfies the ODE (28) after the caustic. Assuming that the following continuity condition on Z (proved in [10]) holds :

$$Z^+(z,y^+(z,x_c(z)))=Z^-(z,y^-(z,x_c(z))), \tag{29}$$

we obtain a uniformly valid formula (except at caustic points) for the energy along a ray :

$$E^\pm(z,y\pm(z,x_0))=\frac{Z^\pm(z,y\pm(z,x_0))}{\partial_z\phi\pm(z,y\pm(z,x_0))|\Theta^\pm(z,y^\pm(z,x_0))|} \tag{30}$$

where $E^\pm$ and $Z^\pm$ are the usual direct/return Eulerian functions (see (23)) and

$$\Theta^\pm(z,y^\pm(z,x_0))=\partial_{x_0}y^\pm(z,x_0).$$

In Eulerian coordinates we have the formulae

$$E^\pm=\frac{Z^\pm}{\Theta^\pm\partial_z\phi^\pm}. \tag{31}$$

which used in (11) eventually gives for any sub-domain D of $\{(x,z)\text{ s.t. }x>0,z>0\}$

$$\int \mathbf{1}_D|A|^2dX\simeq\int \mathbf{1}_{D\cap\mathcal{B}}(\frac{Z^-}{\Theta^-\partial_z\phi^-}+\frac{Z^+}{|\Theta^+|\partial_z\phi^+})dX \tag{32}$$
$$\text{where }\mathcal{B}=\{(x,z)\text{ s.t. }x\le x_c(z)\}$$

3.2 Eulerian equations for Z and Θ

The Lagrangian ODE for $Z(z,y(z,x_0))$ (28) considered as a function of (z,x_0) is given in the previous section. The solution is therefore given by

$$Z(z,y(z,x_0))=Z(0,x_0)\exp(-\int_0^z\frac{\nu}{\partial_z\phi(z,y(z,x_0))}dz)$$

and illustrate the absorption effect of the ν term in (6). As $\nabla_{z,x}\phi^+=\nabla_{z,x}\phi^-$ at the caustic, this formula is correct even across the caustic (thanks to (29)). In particular when $\nu=0$, Z is a constant and this constant is preserved both along the direct and return part of the rays.

We of course apply the Lagrangian to Eulerian transformation of section 2.3 and find a set of two equations for $Z^\pm$:

$$\partial_zZ^\pm+\mathcal{V}^\pm\cdot\partial_xZ^\pm=\frac{\nu}{H(z,x,\partial_x\phi^\pm)}Z^\pm \tag{33}$$

and $Z^-(z, x_c(z)) = Z^+(z, x_c(z))$ on the caustic (use (25)).

Geometrical spreading depends on the evaluation of $\partial_{x_0} y(z, x_0)$. In the ray tracing method, this is done through the linearization of the Hamiltonian system (13) with respect to x_0 (for both direct and return components)

$$\partial_z \begin{pmatrix} \partial_{x_0} y(z, x_0) \\ \partial_{x_0} p(z, x_0) \end{pmatrix} = \begin{pmatrix} H_{xp}(z, y, p) & H_{pp}(z, y, p) \\ -H_{xx}(z, y, p) & -H_{xp}(z, y, p) \end{pmatrix} \begin{pmatrix} \partial_{x_0} y(z, x_0) \\ \partial_{x_0} p(z, x_0) \end{pmatrix} \tag{34}$$

and initial conditions

$$\begin{pmatrix} \partial_{x_0} y(0, x_0) \\ \partial_{x_0} p(0, x_0) \end{pmatrix} = \begin{pmatrix} 1 \\ \partial^2_{x_0^2} \phi_0 \end{pmatrix}$$

As for $\Theta^\pm$ we define $\Lambda^\pm(z, x)$ using the Lagrangian coordinates

$$\Lambda^\pm(z, y(z, x_0^\pm)) = \partial_{x_0} p(z, x_0^\pm)$$

We find (again section 2.3) that they satisfy the Eulerian system of partial differential equation derived from (34) [2],

$$\partial_z \begin{pmatrix} \Theta^\pm \\ \Lambda^\pm \end{pmatrix} + H_p(z, x, \nabla\phi) \cdot \partial_x \begin{pmatrix} \Theta^\pm \\ \Lambda^\pm \end{pmatrix} = \begin{pmatrix} H_{xp}(z, x, \nabla\phi) & H_{pp}(z, x, \nabla\phi) \\ -H_{xx}(z, x, \nabla\phi) & -H_{xp}(z, x, \nabla\phi) \end{pmatrix} \begin{pmatrix} \Theta^\pm \\ \Lambda^\pm \end{pmatrix} \tag{35}$$

with $\Lambda^-(z, x_c(z)) = \Lambda^+(z, x_c(z))$ and necessarily $\Theta^-(z, x_c(z)) = \Theta^+(z, x_c(z)) = 0$ on the caustic.

3.3 Analytical approach to the conjecture

We now define directly $Z^\pm$ by $Z^\pm = E^\pm |\Theta^\pm| \partial_z \phi^\pm$. We also set $T^\pm = |\Theta^\pm| \partial_z \phi^\pm$, then we get

Lemma 1 *When (z,x) in not close to $\mathcal{C}$, we have*

$$\nabla\phi^\pm . \nabla T^\pm = T^\pm \nabla \cdot (\nabla\phi^\pm)$$

Proof. According to the definition of $\theta^\pm$, we have the classical result

$$\partial_z \theta^\pm = \theta^\pm \partial_x \mathcal{V}^\pm$$

In our case ($d = 1$), it is a simple consequence of the relation

$$\partial_z(\partial_{x_0}(y^\pm(z, x_0))) = \partial_{x_0}(\mathcal{V}^\pm(y^\pm(z, x_0))) = \partial_{x_0}(y^\pm(z, x_0)) \frac{\partial \mathcal{V}^\pm}{\partial y}$$

Then, according to relation (24), the Eulerian quantity $\Theta^{\pm}$ satisfies

$$\nabla\phi^{\pm}.\nabla\Theta^{\pm} = \Theta^{\pm}\partial_z\phi^{\pm}\partial_x(\frac{\partial_x\phi^{\pm}}{\partial_{x,z}\phi^{\pm}}) \tag{36}$$

Thus by multiplying by $\partial_z\phi^{\pm}$, we get

$$\partial_z\phi^{\pm}[\nabla\phi^{\pm}.\nabla\Theta^{\pm}] = \Theta^{\pm}\partial_z\phi^{\pm}\nabla\cdot(\nabla\phi^{\pm}) - \Theta^{\pm}\partial_x\phi^{\pm}.\partial_{x,z}\phi^{\pm}$$

Since $\partial_x T^{\pm} = \mp\{\partial_z\phi^{\pm}\partial_x\Theta^{\pm} + \Theta^{\pm}\partial_{x,z}\phi^{\pm}\}$ and $T^{\pm} = \mp\Theta^{\pm}\partial_z\phi^{\pm}$ (we always have $\Theta^{-} \geq 0$ and $\Theta^{+} \leq 0$) we get the desired result.

Proposition 1. *When (z,x) is not close to $\mathcal{C}$, we have*

$$\nu Z^{\pm} + \nabla\phi^{\pm}\nabla Z^{\pm} = 0$$

This equation is exactly the same as (33).

Proof. Multiplying relation (6) by $T^{\pm}$ yields

$$\nu Z^{\pm} + T^{\pm}\nabla.\left(E^{\pm}\nabla\phi^{\pm}\right) = 0$$

Thus we get

$$\nu Z^{\pm} + E^{\pm}T^{\pm}\nabla\cdot(\nabla\phi^{\pm}) + T^{\pm}\nabla E^{\pm}.\nabla\phi^{\pm} = 0.$$

and using the previous lemma we get the result.

4 Computational domain, boundary and initial conditions

One key issue of the problem is the determination of the computational domain as well as Eulerian initial and boundary conditions. The domain is a strip bounded on the $x > 0$ side (should the laser come from the $x < 0$ side) by the caustic curve $x = x_c(z)$ and on the other side by the $x = 0$ axis (see any figure). The physics is indeed trivial in the $x < 0$ half plane where the index is assumed to be constant. We know that the direct $(-)$ solution in this zone is associated to the incident plane wave $A_0\exp(ik_0(z\sin\alpha + x\cos\alpha))$ while the return $(+)$ solution is expected to propagate freely away in the $x < 0$ direction because of the radiation boundary condition imposed on the scattered field. This is the "physical" data we must build on to determine our boundary and initial conditions.

4.1 Boundary conditions

As already mentioned (sections 3.2, 3.3), the boundary conditions on the caustic side all derive from formula (25). All quantities that are transported by the ray flow must match

at the caustic, and in addition geometrical spreading is known to vanish there.

As in [3] all direct $(-)$ quantities are linked to the incident plane wave (2) ; its geometric interpretation forms a uniform set of rays at an angle α with the boundary $x = 0$ (figure 6). It provides - the index of refraction is constant equal to one on the boundary - either a Neumann $\partial_x \phi^- = \cos\alpha$ or a Dirichlet $\phi^- = \phi_{inc} = z \sin\alpha$ boundary condition for the direct phase (see [3] for more details). We recall that $\{\Theta^-(z, y(z, x_0)), \Lambda^-(z, y(z, x_0))\} = \{\partial_{x_0} y(z, x_0), \partial_{x_0} p(z, x_0)\}$ where x_0 is the initial position of the tracked ray $y(z, x_0)$ on the x axis. The resolution of (34) is straightforward in the $x < 0$ where the index of refraction is constant. The solution is constant and its trace on $x = 0$ gives the boundary conditions

$$\Theta^-(z, 0) = 1, \quad \Lambda^-(z, 0) = 0.$$

The quantity Z^- is linked to the incoming amplitude A_0 through formula (31) :

$$Z^- = E^- \Theta^- \partial_z \phi^- = |A_0|^2 \Theta^- \partial_z \phi^- \tag{37}$$

The incident wave models a laser beam of a given thickness that first propagates undisturbed in the $x < 0$ zone, so Z will be zero everywhere on $x = 0$ except on a given window $]z_0, z_1[$ where it simply is one. In practice we use a smoothed (depending on a parameter ϵ) characteristic function :

$$Z^-(z, 0) = |\Xi^\epsilon_{]z_0, z_1[}|^2 \sin\alpha.$$

Like for phase functions, no boundary conditions on $x = 0$ are needed for all return quantities Θ^+, Λ^+ and Z^+ as we assume (a feature of the fold caustic case) that the return flow goes out of our computational domain.

4.2 Initial conditions at $z = 0$

As we already recalled (section 2.2), the localization of the caustic curve depends on a model coupling both the direct and return phases with the caustic equation itself. We therefore need to provide initial Cauchy data for all - direct $(-)$ and return $(+)$ - quantities.

We explained in [3] how to extend the solution to a pseudo-stationary bi-valued model in the $z < 0$ zone (the index is only a priori given $\forall z \geq 0$) that reduces to an easily computable 1-D problem. We then showed that it provides a non interfering Cauchy data for the the system (18) - non interfering here meaning that the stationary solution and the actual solution associated to incident plane wave do not overlap and smoothly connect. It defines in particular an initial caustic point $x_c(0) = C_0$, see figure 6 and [3] for details.

The same strategy applies to the transported quantities above and the initial Cauchy data are given by the solutions $(\Theta_0^\pm, \Lambda_0^\pm)$ of the stationary equations (both for $\pm$ branches)

$$H_p(0,x,\nabla\phi^\pm(0,x))\cdot\partial_x \begin{pmatrix} \Theta_0^\pm \\ \Lambda_0^\pm \end{pmatrix} = \begin{pmatrix} H_{xp}(0,x,\nabla\phi^\pm(0,x)) & H_{pp}(0,x,\nabla\phi^\pm(0,x)) \\ -H_{xx}(0,x,\nabla\phi^\pm(0,x)) & -H_{xp}(0,x,\nabla\phi^\pm(0,x)) \end{pmatrix} \begin{pmatrix} \Theta_0^\pm \\ \Lambda_0^\pm \end{pmatrix}.$$

We know the exact solution to these equations: up to the multiplicative constant C,

$$\begin{aligned} \Theta_0^\pm(x) &= C \mp 2\sqrt{n^2(0,x) - \sin^2\alpha} \\ \Lambda_0^\pm(x) &= C\partial_x(n^2(0,x)). \end{aligned} \tag{38}$$

The constant is determined by the boundary conditions described in section 4.1.

A likewise stationary equation can be used for $Z^\pm$ but, assuming that $Z^-(0,0) = 0$, the initial data $Z_0^\pm$ can be identically set to 0 - the incident energy only flows across the boundary $x = 0, z > 0$.

4.3 Change of variables

We also, as in [3], use the following change of variables

$$\tilde{x}(z,x) = x - x_c(z) + C_0 \tag{39}$$

where C_0 is the position of the caustic of the pseudo-stationary problem in $z < 0$, and thus the initial position $x_c(0) = C_0$ of the caustic. This change of variables simplifies the geometry of our computational domain, and makes its discretization easier. In the new variable $\tilde{x}$, the caustic is simply a straight line $\tilde{x} = C_0$. Setting $\tilde{U}(z,\tilde{x}) = U(z,x)$ in the generic transport equation (24) yields

$$\partial_z\tilde{U} + (H_p(z,\tilde{x} + x_c(z) - C_0, \nabla_{\tilde{x}}\tilde{\phi}) - \dot{x}_c(z))\cdot\nabla_{\tilde{x}}\tilde{U} = f(\tilde{U}(z,\tilde{x}))$$

In particular, in the case of the geometrical spreading, equation (35) rewrites, after change of variables, with simplified notations,

$$\partial_z U + V(z,\tilde{x})\cdot\partial_{\tilde{x}}U = A(z,\tilde{x})U$$

where

$$U = \begin{pmatrix} \tilde{\Theta} \\ \tilde{\Lambda} \end{pmatrix},\ V(z,\tilde{x}) = H_p(z,\tilde{x} + x_c(z) - C_0, \nabla_{\tilde{x}}\tilde{\phi}) - \dot{x}_c(z),$$

$$A(z,\tilde{x}) = \begin{pmatrix} H_{xp}(z,\tilde{x} + x_c(z) - C_0, \nabla_{\tilde{x}}\tilde{\phi}) & H_{pp}(z,\tilde{x} + x_c(z) - C_0, \nabla_{\tilde{x}}\tilde{\phi}) \\ -H_{xx}(z,\tilde{x} + x_c(z) - C_0, \nabla_{\tilde{x}}\tilde{\phi}) & -H_{xp}(z,\tilde{x} + x_c(z) - C_0, \nabla_{\tilde{x}}\tilde{\phi}) \end{pmatrix}$$

More precisely, $\tilde{\Theta}^{\pm}$ and $\tilde{\Lambda}^{\pm}$ are the solutions of

$$\begin{cases} \partial_z U^- + V^-(z,\tilde{x}) \cdot \partial_{\tilde{x}} U^- = A^-(z,\tilde{x}) U^- \\ \partial_z U^+ + V^+(z,\tilde{x}) \cdot \partial_{\tilde{x}} U^+ = A^+(z,\tilde{x}) U^+ \\ U^+(z, x_c(z)) = U^-(z, x_c(z)) \\ + \text{ initial, incoming and outgoing conditions} \end{cases} \tag{40}$$

Remark : Since $\dot{x}_c(z) = H_p(z, x_c(z), p_c(z))$ where $p_c(z) = \partial_x \phi^{\pm}(z, x_c(z))$ (see (18)), the advection fields $V^{\pm}$ vanish at the caustic, which yields the numerical difficulties exposed below. This is not a side effect of the change of variables since it expresses the geometrical fact that at the caustic, the advection fields (which match there see (25)) are parallel to the caustic. More precisely, we proved in [3] that the gradient of the phases $\phi^{\pm}$ behaves as a square root with respect to x in the vicinity of the caustic, i.e. at z fixed

$$\nabla \phi^{\pm}(z,x) = p_c(z) \pm B\sqrt{x_c(z) - x} + O(x_c(z) - x)$$

Plugging this expression into V yields

$$V^{\pm}(z,\tilde{x}) = \pm B\, H_{pp}(z, x_c(z), p_c(z)) \sqrt{C_0 - \tilde{x}} + O(C_0 - \tilde{x}) \tag{41}$$

Strict convexity ensures that $H_{pp} > 0$. This we call the square root behavior of V in the vicinity of the caustic.

5 Numerical scheme for the transport equations

Let $\{\tilde{x}_1, \ldots, \tilde{x}_J\}$ be the regular discretization of $[0, C_0]$. The z discretization $\{z^n\}$ follows by application of a CFL type condition, depending on the angle of the rays with the x-axis (the smaller this angle, the stricter the CFL condition). Let δz and δx be the steps of discretization.

The value of a function a at point $(z^n, \tilde{x}_j)$ is denoted a_j^n, and $\partial_{\tilde{x}}^l a_j^n$ and $\partial_{\tilde{x}}^r a_j^n$ stand for its numerical discrete left and right derivatives. Upwind derivative operators of order 1 are:

$$\partial_{\tilde{x}}^l a_j^n = \frac{a_j^n - a_{j-1}^n}{\delta x}$$
$$\partial_{\tilde{x}}^r a_j^n = \frac{a_{j+1}^n - a_j^n}{\delta x}$$

5.1 Difficulties with the discretization

We focus on the transport of the geometrical spreading (40). The problem of the Z transport equations (33) is similar - in order to illustrate the difficulties involved with the resolution of the transport equations in the vicinity of the caustic.

Let us consider a usual first order explicit discretization of the transport equations (40) as in [4] for instance:

$$\frac{U_j^{n+1} - U_j^n}{\delta z} + V_j^n \cdot \partial_x U|_j^n = A_j^n U_j^n \tag{42}$$

where $\partial_x U|_j^n$ stands for the discrete derivative of U upwinded according to the sign of V_j^n. Convergence studies in [4] generally rely on the assumption that the advection field is constant. In our case, such a discretization fails in the vicinity of the caustic because of the singularity of advection field V (it vanishes at the caustic as a square root as pointed by (41)).

We work with a "stationary" index, independent of z. In this case, we showed in [3] that with appropriate pseudo-stationary boundary conditions, the solution exhibits a vertical caustic, i.e. $\dot{x}_c = 0$ and $p_c = 0$. Then the change of variable (39) has no effect and V is simply H_p. This simplified setting already yields interesting results since it preserves the singularity of V in x.

After removing dependence on z, scheme (42) writes $V_j \cdot \partial_x U|_j = A_j U_j$. At the caustic point $\tilde{x}_J = C_0$, we get $A_J U_J = 0$ since $V_J = 0$. The matrix A_J being invertible (compute H's second derivatives and use $p_c = 0$), this implies $U_J = 0$. Obviously we do not recover the right solution since $U = (\Theta, \Lambda)$ is the Eulerian function corresponding to a non-zero solution of the linear system of ordinary differential equations (34), and therefore does not vanish.

In order to uphold numerically our discussion, we focus on the (stationary) index (44)

$$n(z,x) = \begin{cases} 1 \text{ if } x \leq 0.5 \\ 1 - (x - 0.5)^3 \end{cases}$$

with a pseudo-stationary boundary condition on ϕ

$$\phi_{inc} = z \sin \alpha$$

As explained in [3], the phase ϕ can be computed exactly (up to a constant C ruled by (20)) through

$$\nabla \phi^{\pm} = \mp \sqrt{n^2(0,x) - \sin^2 \alpha} + C$$

Therefore the computations discussed below have been carried out with the exact values of $V = H_p(0, x, \nabla\phi)$, thus proving that the difficulties encountered are not the consequence of errors that might have arisen in the former numerical resolution of the Eikonal equation.

Figure 9 represents, in one dimension, the function Λ^- of x computed using scheme (42) - plain line - and the reference solution (38) - dotted line. As we approach the caustic, the two curves part, and the error is obvious at the caustic since Λ^- does not vanish there whereas scheme (42) produces $U_J = 0$. Increasing the order of the derivative operator to compute $\partial_x U|_j$ does not improve (as shown on figure 10) since $U_J = 0$ still at the caustic.

One can enhance things a little by shifting the computational grid of half a mesh so that the last mesh $x_J = C_0 - \frac{1}{2}\delta x$ is not on the caustic, and $V_J \neq 0$. Figure 11 shows that the solution thus computed does no longer vanish at the caustic, but keeps on parting with the reference solution as one approaches the caustic. This suggests that the local behavior of V

(as a square root) in the vicinity of the caustic, and not only its vanishing, accounts for the numerical difficulties. With second order derivatives, we get the result of figure 12, somehow better, but still far from the accuracy required for the boundary condition on Λ^+ on the caustic derived from (25).

5.2 Numerical scheme

Our proposed solution consists in averaging both the advection field V and the right hand side AU according to the direction of the flow. The scheme writes

$$\frac{U_j^{n+1}-U_j^n}{\delta z}+\frac{1}{2}(V_j^n+V_{j-1}^n)\cdot\frac{U_j^n-U_{j-1}^n}{\delta x}=\frac{1}{2}(A_j^nU_j^n+A_{j-1}^nU_{j-1}^n)$$

when $V_j^n>0$,

$$\frac{U_j^{n+1}-U_j^n}{\delta z}+\frac{1}{2}(V_j^n+V_{j+1}^n)\cdot\frac{U_{j+1}^n-U_j^n}{\delta x}=\frac{1}{2}(A_j^nU_j^n+A_{j+1}^nU_{j+1}^n)$$

when $V_j^n<0$ and simply

$$\frac{U_j^{n+1}-U_j^n}{\delta z}=A_j^nU_j^n$$

when $V_j^n=0$.

We study this scheme in a simplified setting in the annex, and show that it is of order 2 away from the caustic, and degenerates only to order 1 in the vicinity of the caustic. Conversely, the schemes mentioned before degenerate from order 1 or 2 to 0.

Figure 13 shows the reference and the computed solution, which are visually equal. The decisive test, described in section 6.1, is to show that in genuinely 2 dimensional cases, the value of Λ^- we get on the caustic is accurate enough to allow the computation of Θ^+ and Λ^+ through (25).

6 Numerical results

In section 6.1 and 6.2, we compute numerically several functions such as $\Theta^\pm$ and $\Lambda^\pm$, and we check the convergence of our numerical methods as the discretization step tends to 0. We present a pointwise validation of formula (10) in section 6.3. Then we check the theoretical asymptotic results (10) and (11) by letting k_0 to infinity (section 6.4). We add some numerical computations in the case $\nu\neq 0$ in section 6.5.

Let us list several indexes that will be used for our numerical computations. The most simple is the stationary affine index that allows us to compute an analytically exact solution of the Helmholtz equation (1).

$$n^2(z,x) = 1 - x \tag{43}$$

A slightly more realistic stationary index, modeling the propagation in a constant index media before entering the plasma where the ion density increases, is

$$n(z,x) = \begin{cases} 1 \text{ if } x \leq 0.5 \\ 1 - (x - 0.5)^3 \end{cases} \tag{44}$$

In this case we use a finite difference scheme to compute a reference solution of (1). We must however be careful that our verifications are not polluted by the numerical error of this method. We eventually add a z dependence as follows:

$$n(z,x) = \begin{cases} 1 \text{ if } x \leq 0.5 \\ 1 - (1 + 0.2\, z^2)(x - 0.5)^3 \end{cases} \tag{45}$$

and

$$n(z,x) = \begin{cases} 1 \text{ if } x \leq 0.5 \\ 1 - (1 + 0.3 \sin z)(x - 0.5)^3 \end{cases} \tag{46}$$

In this real 2-D case, it is not possible to compute reference solutions of the Helmholtz equation because of the computational cost at high frequencies.

6.1 Order of convergence

We examine the results of the scheme implemented to compute $\Theta^{\pm}$ and $\Lambda^{\pm}$ in a simple setting. We focus again on a pseudo-stationary case, with a (44) type index, but in order to slightly complicate the situation, we tilt the axes at an angle β. More precisely, let us consider the change of coordinates

$$\begin{cases} x = X \cos\beta + Z \sin\beta \\ z = -X \sin\beta + Z \cos\beta \end{cases}$$

and an index of refraction that is stationary with respect to the (Z, X) variable, i.e. depending only on X:

$$n(Z,X) = \begin{cases} 1 \text{ if } X \leq 0.5 \\ 1 - (X - 0.5)^3 \end{cases}$$

We know from the study of stationary cases in [3] that an incoming plane wave induces an outgoing plane wave after touching the caustic, which is not impaired by the change of variables. We therefore expect the outgoing function Λ^+ to vanish when leaving (actually the + part of the rays does leave) the computational domain. Indeed $\partial_{x_0} p = 0$ is a plane waves feature since the direction H_p of the rays is constant.

This will allow us to define the error made in the computation of $\Theta^{\pm}$ and $\Lambda^{\pm}$ as follows. The error on Θ will be the mean value of $|\Theta^-|$ on (a portion limited by z_0 and z_1 of) the caustic (recall that it is supposed to vanish there)

$$\int_{z_0}^{z_1} |\Theta^-(z, x_c(z))| dz \tag{47}$$

and the error on Λ will be the mean value of $|\Lambda^+|$ when leaving the domain at $x = 0$

$$\int_{z_0}^{z_1} |\Lambda^+(z, 0)| dz \tag{48}$$

The numerical results (figures 14 and 15) are computed with $J = 50$ points on the x-axis, an incoming angle $\alpha = \frac{\pi}{4}$, and $\beta = -\frac{\pi}{24}$. We impose $\Theta^- = 1$ and $\Lambda^- = 0$ (plane wave) on the incoming border Γ_{inc}. (The initial conditions are uniformly set to 0, but initial conditions are not a matter of importance with transport equations.) Since we are in a pseudo-stationary case, we only represent our results in one dimension, at constant z. Figure 14 represents the graphs of $\Theta^{\pm}$. Figure 15 shows the graphs of $\Lambda^{\pm}$. Notice the continuity at the caustic.

The array below shows the behavior of the errors (47) and (48) versus the number of points J used to discretize the x-axis. Convergence is of order 1.

Behavior of the errors			
J	50	100	200
On Θ	0.0088	0.0043	0.0021
On Λ	0.0074	0.0038	0.0020

6.2 The energy computations

We now show how our method allows to compute the energy deposited by the laser in a certain domain, that is the integral of E on this domain. Precisely in our bi-valued case, the "geometrical" part of the energy (denoted $\mathbb{E}$) in (11) is the sum of the integrals of E^- and E^+ on the intersection of the domain with the illuminated region.

Using (12) in (11) yields (remember that $E^{\pm} = |a^{\pm}|^2$)

$$\mathbb{E} = \int_D (|a^+|^2 + |a^-|^2) = \int_{\mathbb{D}} \frac{Z^-}{\partial_z \phi^- |\Theta^-|} + \int_{\mathbb{D}} \frac{Z^+}{\partial_z \phi^+ |\Theta^+|}. \tag{49}$$

In our computations below we take for $\mathbb{D}$ the whole computational domain (the illuminated region).

The transport of Z

We consider the index of refraction (45) and take an incoming angle $\alpha = \frac{\pi}{4}$. We solve equation (28) with $\nu = 0$ applying the numerical scheme described in section 5. The incoming condition shown on figure 16 models a laser beam entering the plasma.

Figure 18 represents the contour lines of Z^- and Z^+ superimposed. Notice how the Eulerian resolution of the transport equation (28) renders the corresponding transport along the rays (compare the contour lines of figure 18 with the corresponding rays drawn on figure 17). Indeed, Z is expected to be constant along the rays since $\nu = 0$, therefore the contour lines of Z should be parallel to the rays. However, there is some numerical diffusion, which explains that several contour lines close up instead of being parallel to the rays. On figure 19 we used a Van Leer type second order scheme. There is less numerical diffusion since less contour lines (one actually) close up.

Let us plot the incoming and the outgoing beam on the x-axis. Since Z is constant along the rays ($\nu = 0$), the incoming plateau of figure 16 is expected to be preserved between the two extremal rays, but there is some numerical diffusion. We first take $J = 50$ points discretization in x. On figure 20 we plot the incoming beam, i.e. $Z^-(0, z)$, with dots, and the outgoing beam, i.e. $Z^+(0, z)$, in plain line. On figure 21 the same but using a Van Leer type second order scheme. The plateau is better preserved since the peak reaches 0.85 in the second order case instead of 0.77 in the first order one.

Eventually, figure 22 shows the output of our scheme with $J = 300$ points discretization. Obviously, although converging, our scheme is not adapted for plateau transport (see [5] on this subject). Notice (section 6.1) that our scheme is first order for the transport of the geometrical spreading Θ.

Numerical validation of (49)

We first consider the toy problem with index (43), in which we know the theoretical value $\mathbb{E}_0$ of the integral. We check here the convergence of our numerical method. The array below gives the difference between the computed and the theoretical value of the energy for different values of J.

J	25	50	100
$\mathbb{E}(J) - \mathbb{E}_0$	0.0113	0.0080	0.0056

As expected (see annex 7.3), the convergence is of order $\frac{1}{2}$.

We then return to the 2D case (45) with the incoming condition of figure 16. In that case, we show that the energy we compute converges, although we do not know its exact limit. The array below gives the energy deposited in the whole domain for different values of J. We observe in the table below that the error between two consecutive numerical solutions is first order. We can deduce that we have reached the limit by a 1% margin.

J	25	50	100	200
Energy $\mathbb{E}$	3.1167	3.1000	3.0941	3.0913

6.3 Numerical study of formula (10)

We now present numerical results which use the numerical output of our Eulerian numerical method to approximate the solution A of (1) by (10), still with no absorption. The amplitudes $a\pm$ are given by formula (50) in section 3.1.

The amplitudes $a^{\pm}$ satisfy the real coefficient equations (5) with a possibly complex boundary data. In practice however, we always choose a real positive incoming condition A_0 so that he amplitudes $a^{\pm}$ can be determined by

$$a^{\pm} = \sqrt{E^{\pm}} \tag{50}$$

The first comparison is in our 1-D affine index case (43) for which we have an analytical solution. Figures 23, 24 and 25 plot the real and the imaginary part of both the exact (plain line) and the numerical (stars) solution (as functions of x, z being fixed) for different frequencies. One sees the typical blow up of the GO ansatz at the caustic. Note that only one geometrical optics computation is necessary to compute the approximation (10) for any frequency (indeed the discretization of the GO ansatz – the stars – does not change).

The second comparison is also 1-D but we use the slightly more realistic index (44). This time the "exact" solution of the Helmholtz equation is computed using a given finite difference scheme which is responsible for additional errors. In this case numerical we were only able to compare the modulus of the solution and we now offer an explanation :

Recall that in the 1D case and for $\nu = 0$, $a^+ = a^-$ (see [3]; see also (8)). Then

$$\begin{aligned}
A = \;& a^- e^{-i\pi/4} \exp(ik_0\phi^-) + a^+ e^{i\pi/4} \exp(ik_0\phi^+) \\
= \;& a^- e^{-i\pi/4} (\exp(ik_0\phi^-) + i \exp(ik_0\phi^+)) \\
= \;& a^- e^{-i\pi/4} \exp i(k_0 \tfrac{\phi^+ + \phi^-}{2} + \tfrac{\pi}{4})[\exp i(k_0 \tfrac{\phi^- - \phi^+}{2} - \tfrac{\pi}{4}) + \exp i(k_0 \tfrac{\phi^+ - \phi^-}{2} + \tfrac{\pi}{4})] \\
= \;& 2a^- e^{-i\pi/4} \exp i(k_0 \tfrac{\phi^+ + \phi^-}{2} + \tfrac{\pi}{4}) \cos(k_0 \tfrac{\phi^+ - \phi^-}{2} + \tfrac{\pi}{4})
\end{aligned}$$

Let us consider z fixed. Also remember that in the 1D case, $\frac{\phi^+ + \phi^-}{2}$ is a constant, determined by the phase of the incoming condition (see [3]; see also (9)). We want to emphasize that a numerical error made on the computation of the phases may cause great distortion in a pointwise comparison. Let $\tilde{\phi}^{\pm}$ be the numerical outputs of our method. Let us now choose k_0 such that $k_0 \frac{\tilde{\phi}^+(0) - \tilde{\phi}^-(0)}{2} + \frac{\pi}{4} \equiv \frac{\pi}{2}(2\pi)$, which cancels the real part of the numerical GO ansatz at $x = 0$, and more or less everywhere. Then, because of the numerical error, the real part of the exact solution does not necessarily vanish as we can see on figure 26

($k_0 = 160$).

We thus decide to plot only the moduli of the GO ansatz and the exact solution of the Helmholtz equation. Indeed,

$$|A|^2 = 2|a^-|^2 \cos^2(k_0 \frac{\phi^+ - \phi^-}{2} + \frac{\pi}{4})$$

Now in a pointwise comparison of the moduli, we only get an error on the phase. Figure 27 plots the modulus of the "exact" solution – plain line – versus the modulus of the GO ansatz – stars – for $k_0 = 160$ (compare with figure 26).

Figures 28, 29, 30 are the same for different values of k_0. The phase displacement can be observed for $k_0 = 240$. An analysis is given in the next section.

The last case, with index (46), is a real 2-D case where the caustic is not straight. We only show the GO solution as direct resolutions of (1) are computationally expensive. Figure 32 shows the contour lines of the ansatz (10) evaluated through a computation of the GO problem using 50 points in x. One can observe the compression or dilation effects produced by the heterogeneous plasma.

Notice that the numerical parameter of the method do not depend on k_0. When a finer grid representation of the ansatz is necessary (for high frequencies) the smooth GO parameters can be interpolated on the fine grid.

6.4 Asymptotic convergence

We would like to check numerically the asymptotic convergence predicted by formulae (10) and (11) when $k_0 \to +\infty$. We can do this in the 1-D test cases (43) and (44). One must be careful that the numerical errors in the approximation of the GO solution does not pollute the asymptotic error. In other words we must make sure that this error, depending on δx, is less than $O(k_0^{-1})$ for (10) and $O(k_0^{-1/3})$ for (11).

Formula (10)

Let A be the exact solution to (1). Let A^{k_0} be its geometrical optics approximation in (10),

$$A^{k_0} = \frac{C}{2\sqrt{\pi}}\{a^- e^{-i\pi/4} \exp(ik_0\phi^-) + a^+ e^{i\pi/4} \exp(ik_0\phi^+)\}$$

Formula (10) claims that, away from the caustic,

$$\|A - A^{k_0}\| = O(k_0^{-1})$$

where $\|.\|$ is the L^∞ norm in a closed region not containing the caustic.

Let $h = \delta x$ be our discretization step. We denote by $\phi_h^\pm$ and $a_h^\pm$ the outputs of our numerical scheme. We showed in [3] (for ϕ) and in this paper (for a) that the numerical approximations are of order 1 :

$$\|\phi^\pm - \phi_h^\pm\| = O(h)$$
$$\|a^\pm - a_h^\pm\| = O(h)$$

We finally denote by $A_h^{k_0}$ the numerical geometric optics approximation of A,

$$A_h^{k_0} = \frac{C}{2\sqrt{\pi}}\{a_h^- e^{-i\pi/4}\exp(ik_0\phi_h^-) + a_h^+ e^{i\pi/4}\exp(ik_0\phi_h^+)\}$$

The numerical error made in the approximation of $a\exp(ik_0\phi)$ by $a_h\exp(ik_0\phi_h)$ is

$$\begin{aligned} |a\exp(ik_0\phi) \quad & -a_h\exp(ik_0\phi_h)| \\ & \leq |(a-a_h)\exp(ik_0\phi)| + |a_h(\exp(ik_0\phi) - \exp(ik_0\phi_h))| \\ & \leq O(h) + |a_h\exp(ik_0\phi)| \cdot |1 - \exp(ik_0(\phi_h - \phi))| \\ & \leq O(h) + O(1 - \exp(ik_0 O(h))) \\ & \leq O(h) + O(hk_0) \end{aligned}$$

assuming that $hk_0 \to 0$. Therefore, summing on $\pm$ gives

$$\|A^{k_0} - A_h^{k_0}\| \leq O(h) + O(hk_0)$$

We are interested in the convergence of $A_h^{k_0}$ towards A, so we consider

$$\begin{aligned} \|A - A_h^{k_0}\| \quad & \leq \|A - A^{k_0}\| + \|A^{k_0} - A_h^{k_0}\| \\ & \leq O(k_0^{-1}) + O(h) + O(hk_0) \end{aligned}$$

Theoretically, taking $h = O(k_0^{-2})$ would allow to observe a convergence of $A_h^{k_0}$ towards A of order

$$\|A - A_h^{k_0}\| \leq O(k_0^{-1})$$

In practice, our Matlab cannot afford a $h = O(k_0^{-2})$ discretization for large values of k_0. Given reasonable values of $h \sim 10^{-2}$, for large k_0 the $O(hk_0)$ error is too important, and for smaller k_0 the $O(k_0^{-1})$ error becomes important.

We nevertheless give numerical results in the array below, computed with the (43) index, showing the errors as a function of k_0. The error is the maximum point-wise error away from the caustic where we know (10) to be inaccurate. We chose to privilege large values of k_0, thus causing a large $O(hk_0)$ error. Note this time that we must rerun the GO computation for each k_0 evaluation.

k_0	J	$\|A - A_h^{k_0}\|$	$\|A - A^{k_0}\|$	$\|A^{k_0} - A_h^{k_0}\|$
200	50	0.1412	0.0422	0.1465
400	200	0.0363	0.0287	0.0360

The error made in the numerical approximation of A^{k_0} by $A_h^{k_0}$, due to the $O(hk_0)$ term, is much larger than the geometric optics approximation theoretical $O(k_0^{-1})$ error for $k_0 = 200$ and $J = 50$. On the next step, where $k_0 = 400$ and $J = 200$, both errors are comparable. Unfortunately, are not able to compute the following step that would be $k_0 = 800$ and $J = 800$, which should allow to observe the $O(k_0^{-1})$ error in $\|A - A_h^{k_0}\|$. Eventually, notice that the range of k_0 is yet too small to observe a truly $O(k_0^{-1})$ convergence of $\|A - A^{k_0}\|$ (the error is not quite divided by 2).

In the second 1-D case (44), we no longer know the theoretical values of the asymptotic approximation A^{k_0} of A. However, $\|A - A_h^{k_0}\| \leq O(k_0^{-1}) + O(h) + O(hk_0)$ still holds. Notice that the $h = O(k_0^{-2})$ discretization imposed to prevent numerical errors from polluting the asymptotic approximation is stricter than the $h = O(k_0^{-1})$ discretization required for the computation of the exact solution of the Helmholtz equation (1) using a finite difference scheme.

The $O(h)$ error comes from the numerical error made in the computation of the amplitudes, whereas the $O(hk_0)$ error is due to the numerical error on the phases. In this case, the error we make in the computation of the phase is such that, for reasonable values of $h \sim 10^{-2}$, the $O(hk_0)$ error is too large to allow a pointwise comparison. Indeed, figure 31 compares the GO ansatz, computed with a $J = 200$ points discretization in x, and the "exact" solution of the Helmholtz equation for $k_0 = 60$. Even at this low frequency, results are not visually satisfactory (check the extremal points of the imaginary part). The array below still gives numerical results. As pointed out, the errors are larger than in the (43) case.

k_0	J	$\|A - A_h^{k_0}\|$
200	50	0.6179
400	200	0.3419

Formula (11)

The discretization error in (49) being of order $\frac{1}{2}$, we need $\sqrt{\delta x} = O(k_0^{-1/3})$ to verify (11). We take $\delta x = k_0^{-2/3}$. The array below shows the difference between the energy of the solution A of (1), that is the integral of $|A|^2$, and the output of our numerical scheme. Both converge towards the exact value of (49), but we check the rate of convergence, which is indeed found to be of order $O(k_0^{-1/3})$.

k_0	125	350	1000
Error	0.0114	0.0080	0.0056

6.5 A $\nu \neq 0$ case

We eventually give numerical results in a case with absorption. We take $\nu = \nu_0 N$ with $\nu_0 = 0.7$. We consider the incoming beam of figure 16 propagating in the (45) index. Figure

33 represents the contour lines of Z^- and Z^+ superimposed. Notice how Z diminishes in the vicinity of the caustic (where the electronic density N and thus the absorption coefficient ν are the highest). Indeed, four contour lines close up instead of one (due to numerical diffusion) in the no absorption case of figure 19. Figure 34 represents the numerical realization of ansatz (10). One checks both the energy concentration in the vicinity of the caustic and the absorption effect of the plasma.

7 Annex

7.1 The toy problem with an linear profile of n^2

We assume here that the simulation domain is the strip $x \in [0,1]$, that the absorption coefficient ν is constant and that the incident wave is entering into the domain at $x = 0$ with an incidence angle equal to α. Since the problem is invariant according to the z direction, we seek a solution to the initial Helmholtz in the form $A(x,z) = u(x)e^{ik_0 z \sin\alpha}$. Then we have to consider the equation

$$u''(x) + k_0^2(x_c - x)u(x) + ik_0\nu u = 0 \tag{51}$$

with $x_c = \cos^2\alpha$. According to the form of the incident wave, the boundary condition for u in $x = 1$ reads as

$$\left[iuk_0\cos\alpha - \frac{\partial u}{\partial x}\right]_{x=0} = 2ik_0\cos\alpha$$

The absorbed energy in an interval $[x_1, x_2]$ is equal to $\nu\mathcal{H}_{x_1,x_2}$, where

$$\mathcal{H}_{x_1,x_2} = \int_{x_1}^{x_2} |u(x)|^2 dx$$

On the other hand, the Eikonal equation may be written here

$$|\frac{\partial\phi^\pm}{\partial x}|^2 + |\frac{\partial\phi^\pm}{\partial z}|^2 = \frac{x}{L}.$$

Since we have $\frac{\partial\phi^-}{\partial z} = \frac{\partial\phi+}{\partial x} = \sin\alpha$, we get

$$\frac{\partial\phi^-}{\partial x} = -\sqrt{x_c - x}, \quad \frac{\partial\phi^+}{\partial x} = \sqrt{x_c - x}$$

Since $\Theta^\pm$ is solution to $\partial_x\Theta^\pm = \Theta^\pm\partial_x(\partial_x\phi^\pm)(\partial_x\phi^\pm)^{-1}$, we see that it is proportional to $\partial_x\phi^\pm$ and we get

$$\Theta^- = |\Theta^+| = \sqrt{\frac{x_c - x}{x_c}},$$

Now, the equation for $Z^{\pm}$ reads as:

$$\nu Z^- - \sqrt{x_c - x}\frac{\partial Z^-}{\partial x} = 0, \quad Z^-(0) = 1$$

$$\nu Z^+ + \sqrt{x_c - x}\frac{\partial Z^+}{\partial x} = 0, \quad Z^+(x_c) = Z^-(x_c)$$

whose solutions are

$$\begin{aligned} Z^-(x) &= \exp\left(-2\nu\sqrt{x_c} + 2\nu\sqrt{x_c - x}\right) \\ Z^+(x) &= \exp\left(-2\nu\sqrt{x_c} - 2\nu\sqrt{x_c - x}\right) \end{aligned}$$

Then we get

$$\frac{Z^-}{\Theta^-} + \frac{Z^+}{|\Theta^+|} = 2e^{-2\nu\cos\alpha}\sqrt{\frac{x_c}{x_c - x}}\cosh(2\nu\sqrt{x_c - x})$$

Proposition For any x_1, x_2 in the interval $[0, x_c]$, we have then k_0 goes to infinity.

$$\mathcal{H}_{x_1,x_2} \simeq \int_{x_1}^{x_2}\left(\frac{Z^-}{\Theta^-} + \frac{Z^+}{|\Theta^+|}\right)dx \tag{52}$$

Let us first state the following technical result.

Lemma 1

For ζ real positive number going to ∞ and ω positive real number bounded, we have :

$$|\left(\mathbf{Ai}(-(\zeta + i\omega)\right)|^2 = \zeta^{-1/2}\frac{1}{2\pi}\left(\cosh(2\zeta^{1/2}\omega) - \sin(\frac{4}{3}\zeta^{3/2})\right)(1 + o(\zeta^{-1}))$$

Proof of the proposition

We set

$$w(\zeta) = u(x), \qquad \zeta = (x_c - x)k_0^{2/3}$$

If we denote $\widehat{\nu} = \nu k_0^{-1/3}$ and $\zeta_L = (\cos^2\alpha)k_0^{2/3}$, equation (51) may be written as

$$w'' + \zeta w + i\widehat{\nu}w = 0, \tag{53}$$

$$[w + \frac{ik_0^{-1/3}}{\cos\alpha}\frac{\partial w}{\partial \zeta}]_{\zeta_L} = 2 \tag{54}$$

The only "physical" solution (that is compatible with the radiation boundary condition) is the following Airy function

$$w(\zeta) = Ck_0^{1/6}\mathbf{Ai}(-\zeta - i\widehat{\nu}), \tag{55}$$

$$u(x) = Ck_0^{1/6}\mathbf{Ai}(-k_0^{2/3}(x_c - x) + \nu k_0^{-1/3}) \tag{56}$$

According to the boundary condition (54), we will now evaluate the constant C. According to the classical asymptotic expansion of the Airy function (see e.g. [1]), we know that

$$w(\zeta) \simeq \frac{Ck_0^{1/6}}{\sqrt{\pi}(\zeta + i\widehat{\nu})^{1/4}}\sin(\frac{2}{3}(\zeta + i\widehat{\nu})^{3/2} + \frac{\pi}{4})$$

$$(\partial_\zeta w)(\zeta) \simeq \frac{Ck_0^{1/6}}{\sqrt{\pi}(\zeta + i\widehat{\nu})^{1/4}}\cos\left(\frac{2}{3}(\zeta + i\widehat{\nu})^{3/2} + \frac{\pi}{4}\right)(\zeta + i\widehat{\nu})^{1/2}$$

Since $(\zeta_L + i\widehat{\nu})^{1/4} = (\cos\alpha)^{1/2}k_0^{1/6}(1 + O(k_0^{-1}))$, we get

$$[w + \frac{ik_0^{-1/3}}{\cos\alpha}(\partial_\zeta w)]_{\zeta_L} \simeq$$
$$\frac{C}{\sqrt{\pi}\cos^{1/2}\alpha}\left(\sin[\frac{2}{3}(\zeta_L + i\widehat{\nu})^{3/2} + \frac{\pi}{4}] + i\cos[\frac{2}{3}(\zeta_L + i\widehat{\nu})^{3/2} + \frac{\pi}{4}]\right)$$

Now according to the condition (54) we must have

$$4 = \frac{|C|^2}{\pi\cos\alpha}|\exp(-i\frac{2}{3}(\zeta_L + i\widehat{\nu})^{3/2})|^2 = \frac{|C|^2}{\pi\cos\alpha}\exp(\frac{4}{3}\mathrm{Im}((\zeta_L + i\widehat{\nu})^{3/2}))$$

Since $\zeta_L^{1/2}\widehat{\nu} = \nu\cos\alpha$,we see according to (59) that,

$$|C|^2 = 4\pi e^{-2\nu\cos\alpha}\cos\alpha \tag{57}$$

Now, we focus on the evaluation of $\mathcal{H}_{x_1,x_2}$. According to Lemma 1, we see that for any x_1, x_2 smaller than x_c:

$$\mathcal{H}_{x_1,x_2} = k_0^{1/3}\int_{x_1}^{x_2} C^2|\mathbf{Ai}(-(x_c - x)k_0^{2/3} - i\widehat{\nu})|^2 dx$$
$$\simeq \frac{C^2}{2\pi}\int_{x_1}^{x_2}(x_c - x)^{-1/2}\Big(\cosh[2((x_c - x)k_0^{2/3})^{1/2}k_0^{-1/3}\nu]$$
$$-\sin[\frac{4}{3}k_0(x_c - x)^{3/2}]\Big)\,dx$$

thus

$$\mathcal{H}_{x_1,x_2} \simeq \frac{C^2}{2\pi}\int_{x_1}^{x_2}\sqrt{\frac{x_c}{x_c-x}}\cosh[2\nu(x_c-x)^{1/2}]dx$$

That is to say (52).

Proof of the lemma. We know, according to [1] for example, that

$$\mathbf{Ai}(-(\zeta+i\omega)) = \frac{(\zeta+i\omega)^{-1/4}}{\sqrt{\pi}}\sin(\frac{2}{3}(\zeta+i\omega)^{3/2}+\pi/4)(1+o((\zeta+i\omega)^{-1})). \tag{58}$$

Thus we get

$$|\mathbf{Ai}(-(\zeta+i\omega))|^2 = \frac{(\zeta+i\omega)^{-1/2}}{2\pi}\left(\cosh(\frac{4}{3}\mathrm{Im}((\zeta+i\omega)^{3/2}) + \sin(\frac{4}{3}\mathrm{Re}((\zeta+i\omega)^{3/2}))\right)(1+o(\zeta^{-1})).$$

Since we have :

$$\mathrm{Im}((\zeta+i\omega)^{3/2}) = |\zeta^2+\omega^2|^{3/2}\sin(\frac{3}{2}\mathrm{arctg}\frac{\omega}{\zeta}) = \frac{3}{2}\zeta^{1/2}\omega(1+o(\zeta^{-1})) \tag{59}$$
$$\mathrm{Re}((\zeta+i\omega)^{3/2}) = \zeta^{3/2}(1+o(\zeta^{-1})),$$

we see that :

$$\cosh(\frac{4}{3}\mathrm{Im}((\zeta+i\omega)^{3/2})+\sin(\frac{4}{3}\mathrm{Re}((\zeta+i\omega)^{3/2})) \simeq \left(\cosh(2\zeta^{1/2}\omega)+\sin(\frac{4}{3}\zeta^{3/2})\right)(1+o(\zeta^{-1}))$$

Thus the desired result. $\diamond$

Remark

As it was indicated in the introduction, we check that the solution to equation (51) given by (56) satisfies for $x < x_c$, as $k_0 \to +\infty$, the following approximation

$$u(x) \simeq a^+ e^{-i\pi/4}\exp(ik_0\phi^+) + a^- e^{+i\pi/4}\exp(-ik_0\phi^-)$$

where

$$a^\pm = \frac{1}{(x_c - x + i\nu k_0^{-1})^{1/4}}$$

and $\phi^\pm$ is given above

7.2 Order of the scheme

We focus on a simplified transport equation (24), depending only on x, of the form

$$v(x)f'(x) = a(x)f(x) \tag{60}$$

where $v(x) \geq 0$. We study different numerical schemes to solve this equation, keeping in mind that in order to ensure stability, we use only upwind schemes. For each scheme, we first determine its order in the case where v is smooth. We then study the behavior of the remainder near the caustic in the case where $v(x)$ behaves as a square root as in (41). In that case we denote

$$v(x) = \sqrt{x_c - x}\, w(x)$$

Scheme 1:

$$v(x)\frac{f(x) - f(x-h)}{h} = a(x)f(x)$$

Order of this scheme:

$$v(x)\frac{f(x) - f(x-h)}{h} - a(x)f(x) = -\frac{1}{2}f(x)R_1(x)h + O(h^2)$$

where

$$R_1(x) = \frac{a'(x)v(x) - a(x)v'(x) + a(x)^2}{v(x)}$$

When $v(x)$ behaves as a square root,

$$R_1(x) = \frac{2(x - x_c)(a(x)w'(x) + a'(x)w(x)) + 2\sqrt{x_c - x}a(x)^2 + a(x)w(x)}{2w(x)(x_c - x)}$$

and as $h \to 0$,

$$R_1(x_c - h)h \to \frac{a(x_c)}{2}$$

Using the same heuristic argument as in [3], we claim that if a does not vanish at the caustic, this scheme does not converge as one approaches the caustic, since the remainder is of order $O(1)$.

We study next a second order scheme, but as we shall see, it still does not converge at the caustic.

Scheme 2:

$$v(x-\frac{1}{2}h)\frac{f(x)-f(x-h)}{h}=a(x-\frac{1}{2}h)\frac{f(x)+f(x-h)}{2}$$

Order of this scheme:

$$v(x-\frac{1}{2}h)\frac{f(x)-f(x-h)}{h}-a(x-\frac{1}{2}h)\frac{f(x)+f(x-h)}{2}$$
$$=-\frac{1}{24}f(x)R_2(x)h^2+O(h^3)$$

where

$$R_2(x)=(6a'(x)a(x)v(x)+2a(x)^3+2a''(x)v(x)^2$$
$$+2a'(x)v'(x)v(x)+a(x)v''(x)v(x)-2a(x)v'(x)^2)/v(x)^2$$

In the case where $v(x)$ behaves as a square root, the leading terms in R_2 are $v''v$ and v'^2: as $x\to x_c$,

$$R_2(x)\simeq a(x)\frac{v''(x)v(x)-2v'(x)^2}{v(x)^2}$$

and as $h\to 0$,

$$R_2(x_c-h)h^2\to -\frac{3}{4}a(x_c)$$

Again, if a does not vanish at the caustic, this scheme does not converge as one approaches the caustic.

We now study the scheme proposed in this article (section 5.2), and show that the remainder remains of order 1 as we approach the caustic.

Scheme 3:

$$\frac{v(x)+v(x-h)}{2}\frac{f(x)-f(x-h)}{h}=\frac{a(x)f(x)+a(x-h)f(x-h)}{2}$$

Order of this scheme:

$$\frac{v(x)+v(x-h)}{2}\frac{f(x)-f(x-h)}{h}-\frac{a(x)f(x)+a(x-h)f(x-h)}{2}$$
$$=-\frac{1}{12}f(x)R_3(x)h^2+O(h^3)$$

where

$$R_3(x) = (3a'(x)a(x)v(x) + a(x)^3 + a''(x)v(x)^2 + a'(x)v'(x)v(x) - a(x)v''(x)v(x) - a(x)v'(x)^2)/v(x)^2$$

For this scheme, in the case where $v(x)$ behaves as a square root, the key ingredient is that the leading terms $v''v$ and v'^2 simplify: $v''(x)v(x) + v'(x)^2 = 0$. Then

$$R_2(x) \simeq \frac{a(x)^3 + a'(x)v'(x)v(x)}{v(x)^2}$$

and as $h \to 0$,

$$R_2(x_c - h)h^2 = O(h)$$

7.3 Numerical integration

Of course the main difficulty here is that $\Theta^{\pm}$ vanishes at the caustic. Let us consider the toy problem (43), and study how the integral (49) behaves through discrete integration of the exact function sampled at a δx step. Solving (35) we get

$$\Theta^{\pm}(x) = \pm\frac{\cos\alpha}{\sqrt{\cos^2\alpha - x}}$$

With proper boundary conditions, $\partial_x\phi^{\pm}$ and $Z^{\pm}$ are constant. Then up to a constant,

$$\mathbb{E} = \int_0^{\cos^2\alpha} \frac{1}{\sqrt{\cos^2\alpha - x}}dx$$

We focus on the simplified formula

$$\mathbb{E} = \int_0^1 \frac{1}{\sqrt{x}}dx$$

Let us study the convergence of the discrete integral

$$\mathbb{E}_n = \frac{1}{n}\sum_{k=1}^{n} \frac{1}{\sqrt{\frac{k}{n}}}$$

Since $x \mapsto \frac{1}{\sqrt{x}}$ decreases, we get

$$\int_{\frac{1}{n}}^{1+\frac{1}{n}} \leq \mathbb{E}_n \leq \int_0^1 \frac{1}{\sqrt{x}}dx$$

and therefore

$$|\mathbb{E} - E_n| = O(\sqrt{\frac{1}{n}})$$

In the general case, in order to improve the precision, we use a specific evaluation in the last mesh and a trapezoidal interpolation elsewhere, but as we shall see we did not manage to remove this $O(\sqrt{\delta x})$ behavior.

References

[1] M. Abramowitz and I. A. Stegun *Handbook of mathematical functions with formulas, graphs, and mathematical tables* Dover, New York, 1992; MR 94b:00012

[2] J.-D. Benamou. Direct solution of multi-valued phase-space solutions for hamilton-jacobi equations. *Comm. Pure Appl. Math.*, 52, 1999.

[3] J.-D. Benamou, O. Lafitte, R. Sentis and I. Solliec. A geometric optics method for high frequency electromagnetic fields computations near fold caustics - Part I. *submitted.*

[4] R. Dautray and J. L. Lions. Mathematical Analysis and Numerical Methods for Science and Technology, Vol. 6. *Springer*, 1993.

[5] B. Després and F. Lagoutière J. Sci. Comput. **16** (2001), no. 4, 479–524 (2002).

[6] J.J. Duistermaat. Oscillatory integrals, lagrange immersions and unfolding of singularities. *Comm. Pure Appl. Math.*, 27:207–281, 1974.

[7] M. V. Fedoryuk. *Partial Differential Equations (Chap. 1).* Springer-Verlag, 1988.

[8] W.L. Kruer. *The phycics of Laser Plasma Interactions.* Addison-Wesley, New york (1988). *Laser Plasma Interaction.*

[9] O. Lafitte and I. Solliec *in preparation.*

[10] I. Solliec *PhD dissertation.*

[11] D. Ludwig. Uniform asymptotic expansions at a caustic. *Comm. Pure Appl. Math.*, 19:215–250, 1966.

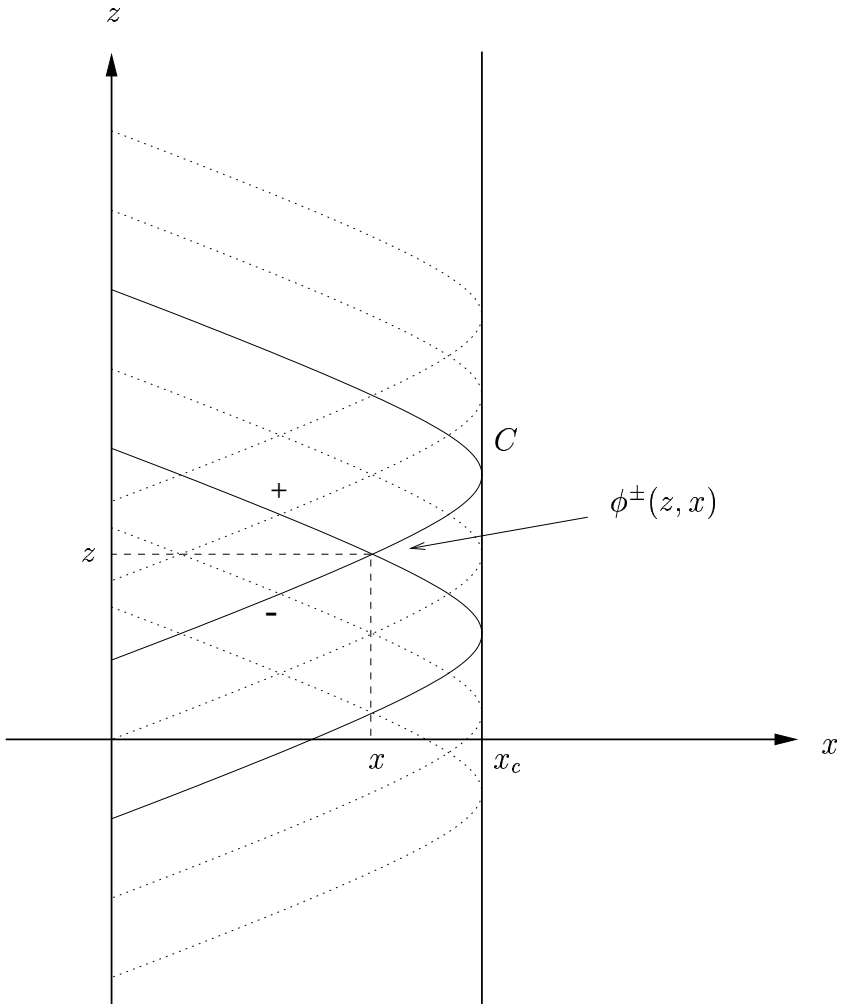

Figure 1: The toy problem

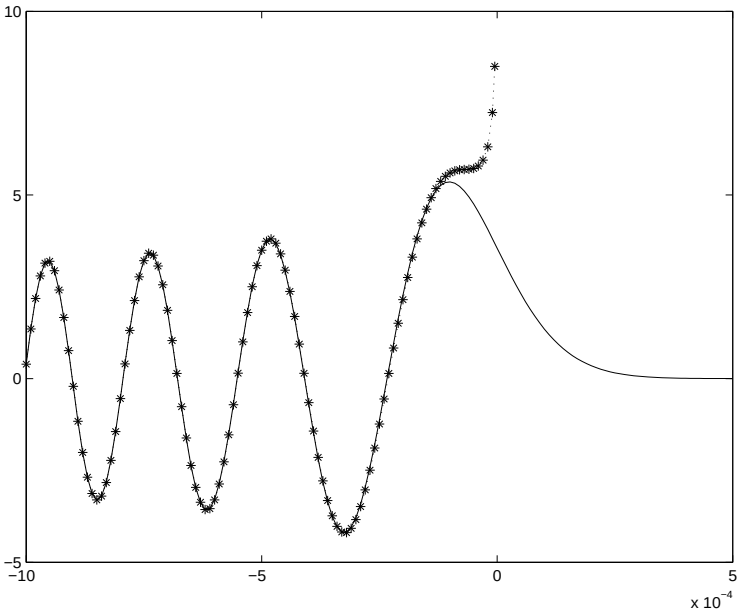

Figure 2: The Airy function and its approximation

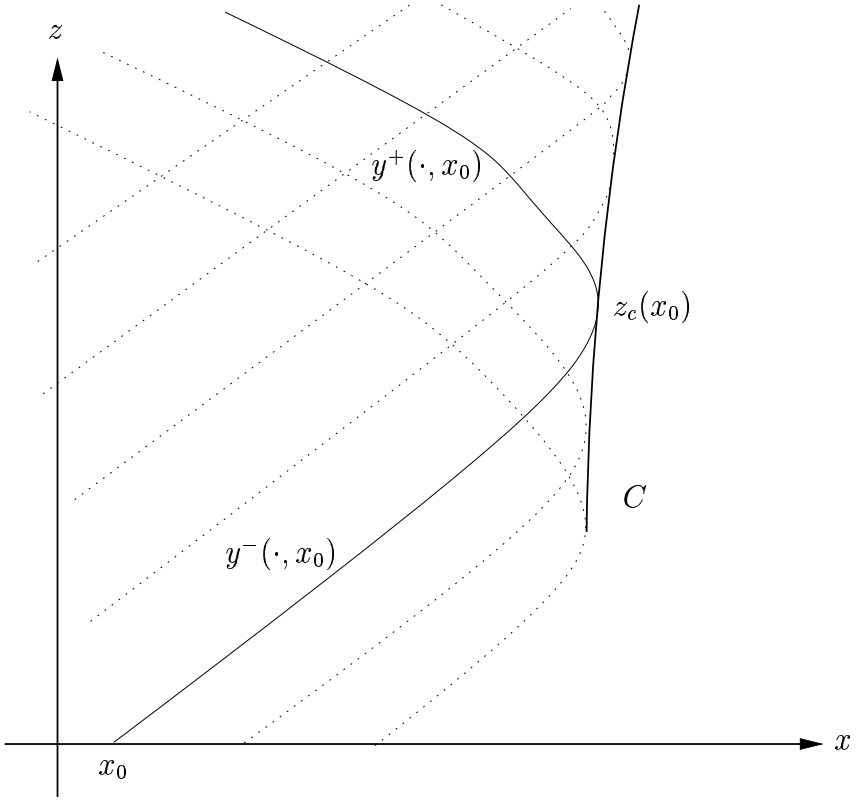

Figure 3: The $y^{\pm}$ splitting

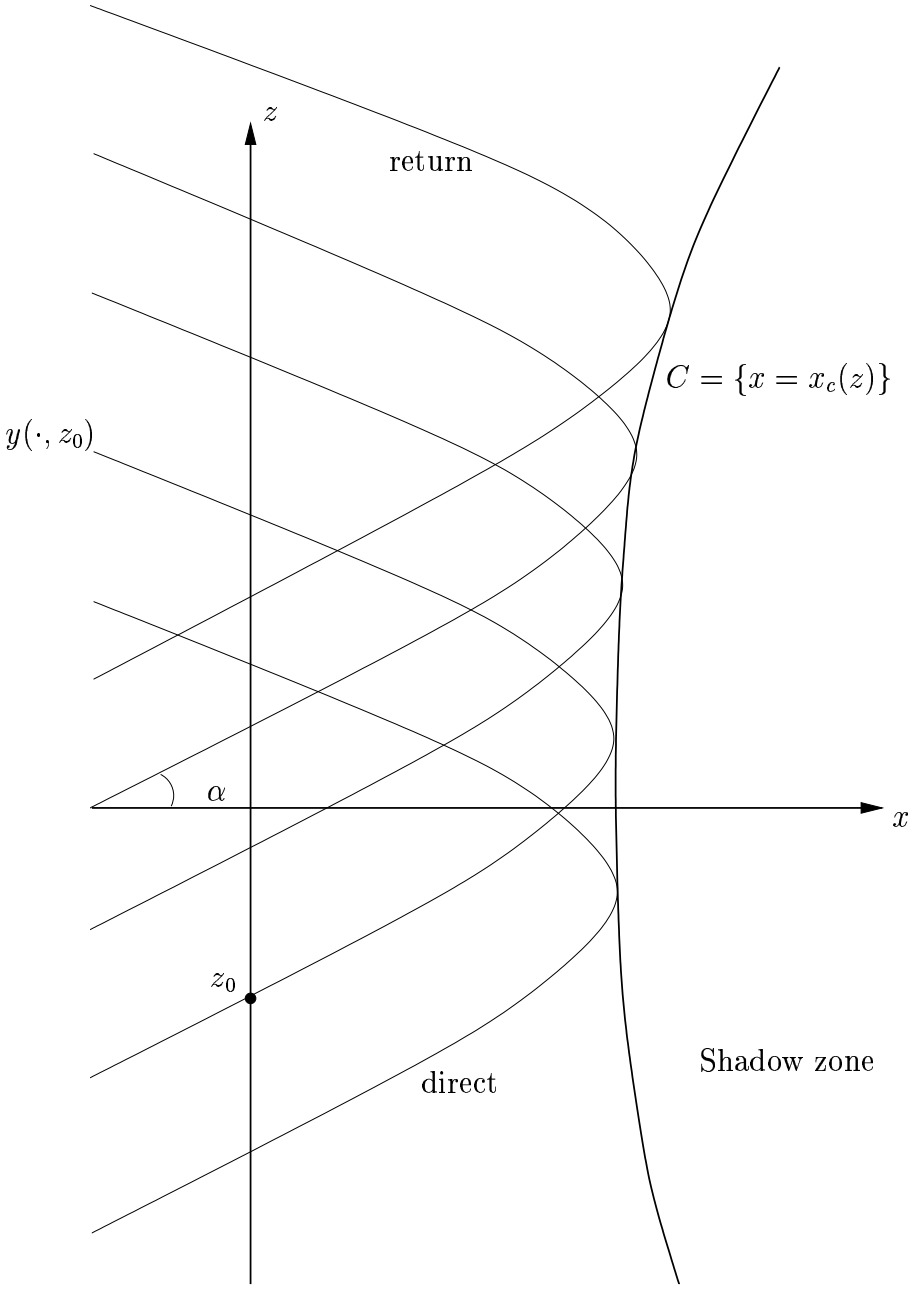

Figure 4: The infinite model

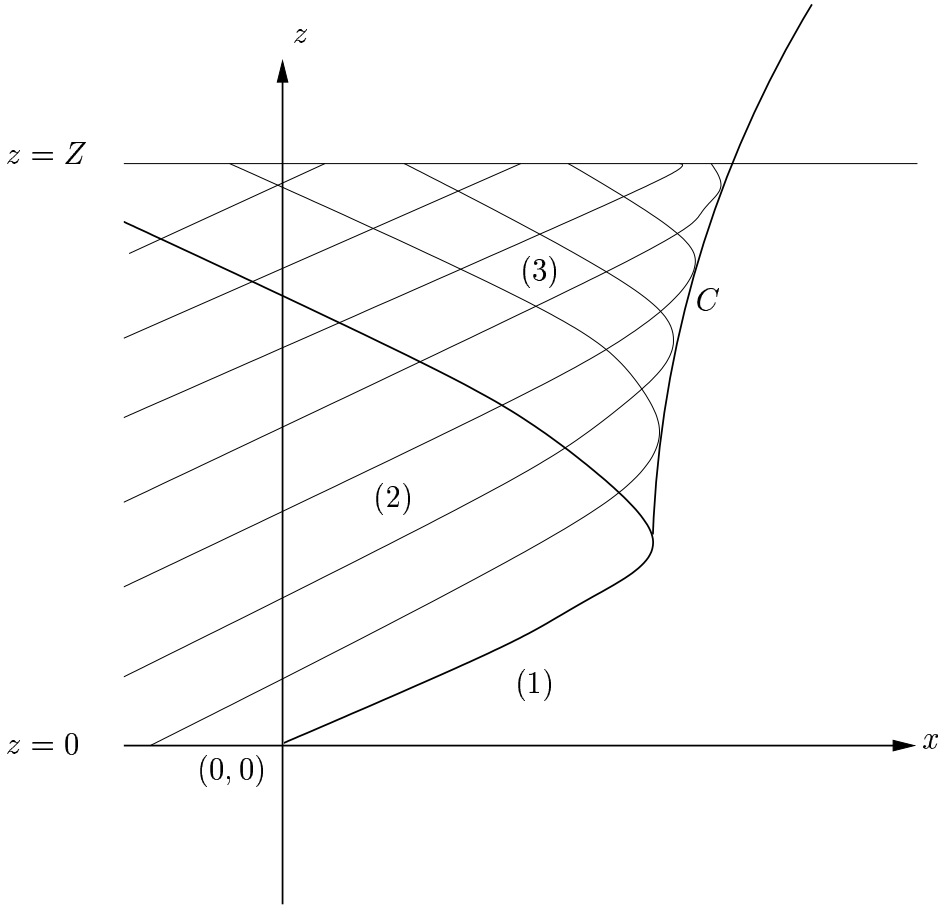

Figure 5: The bounded model

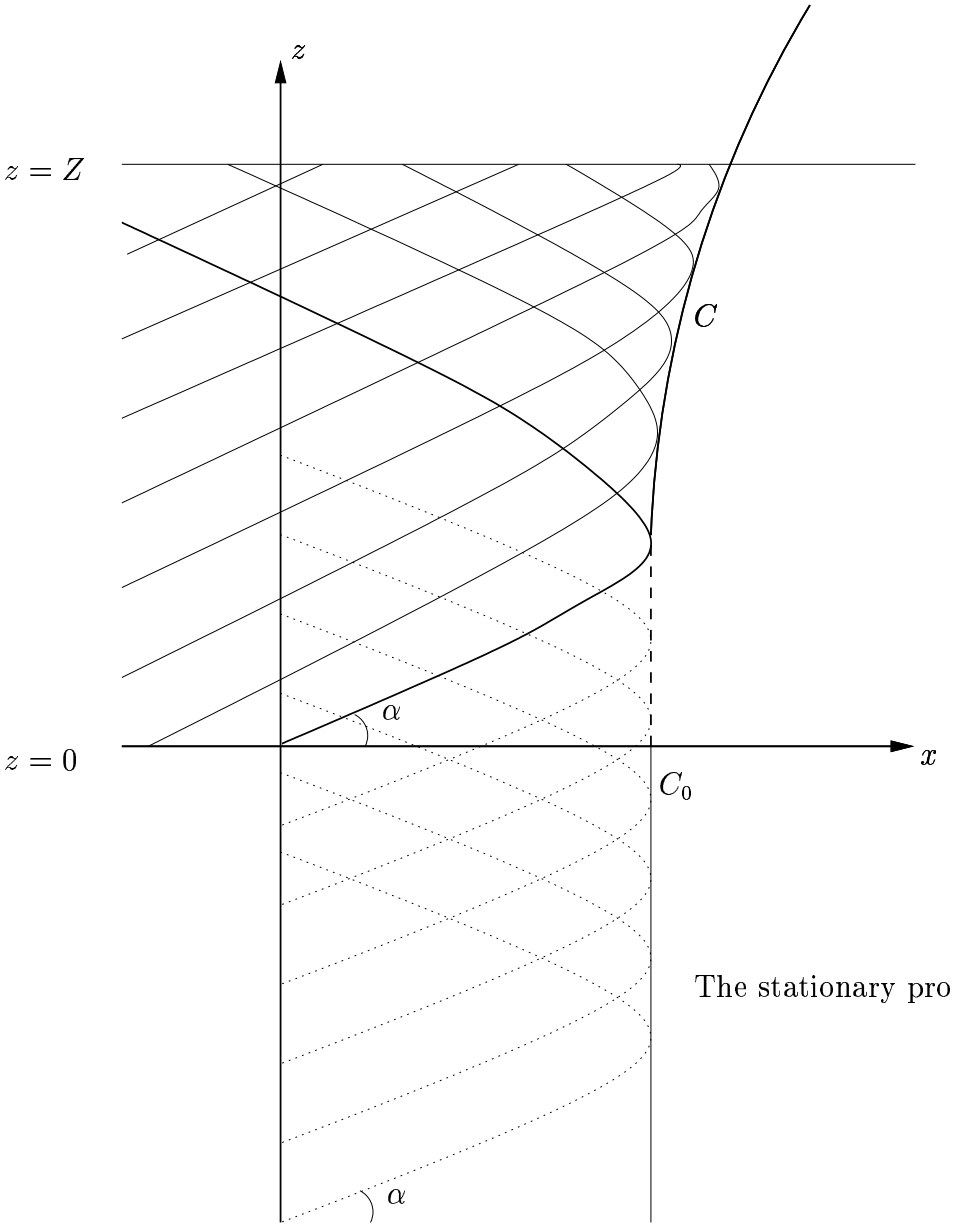

Figure 6: Initialization by a stationary problem

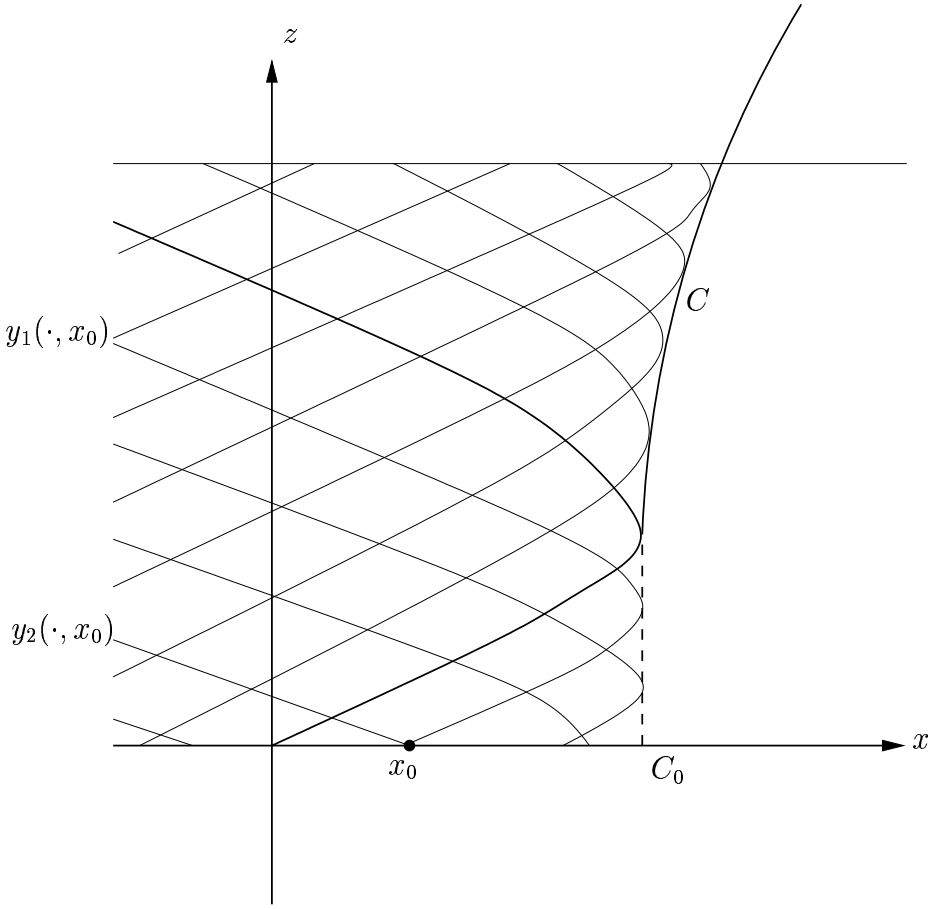

Figure 7: The full bounded model

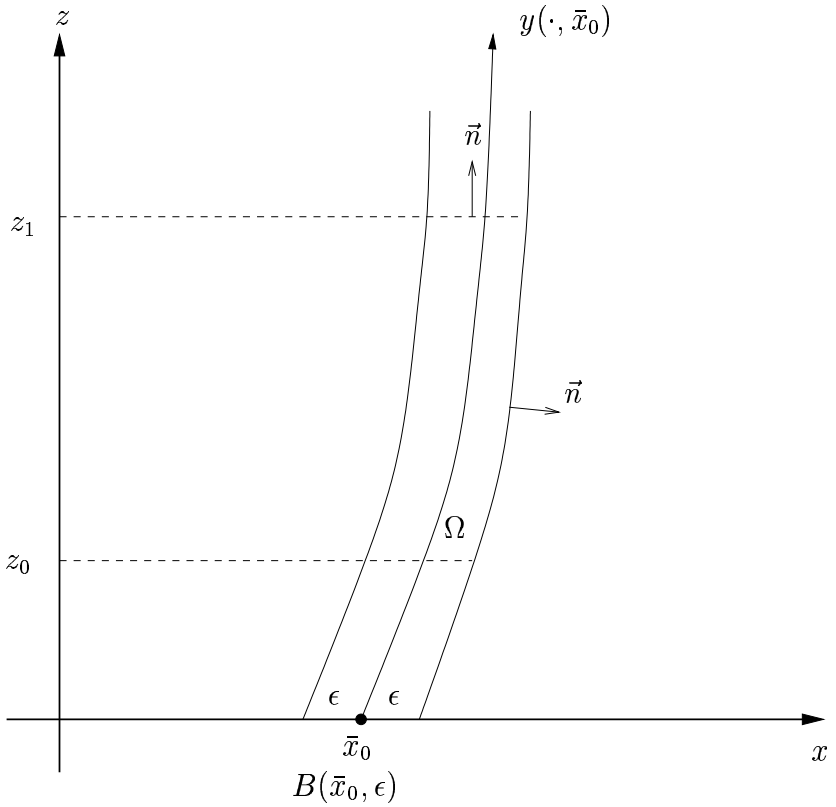

Figure 8: A tube of rays

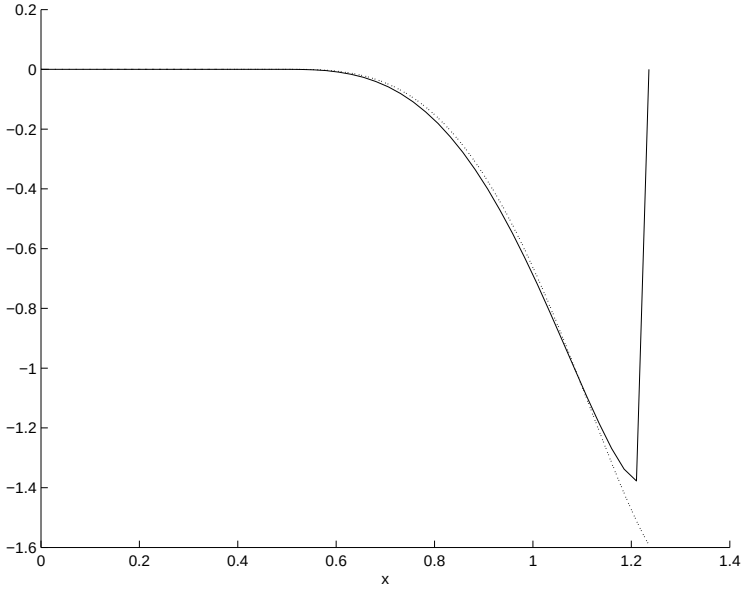

Figure 9: Order 1 scheme

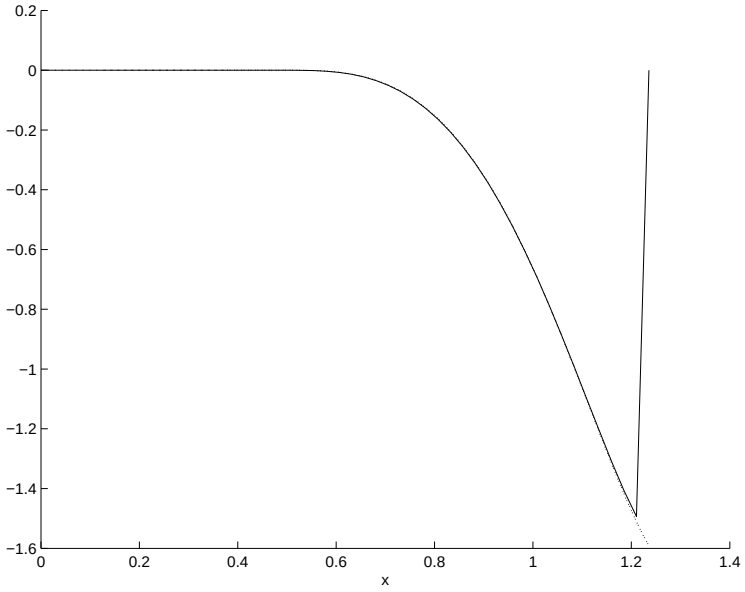

Figure 10: Order 2 scheme

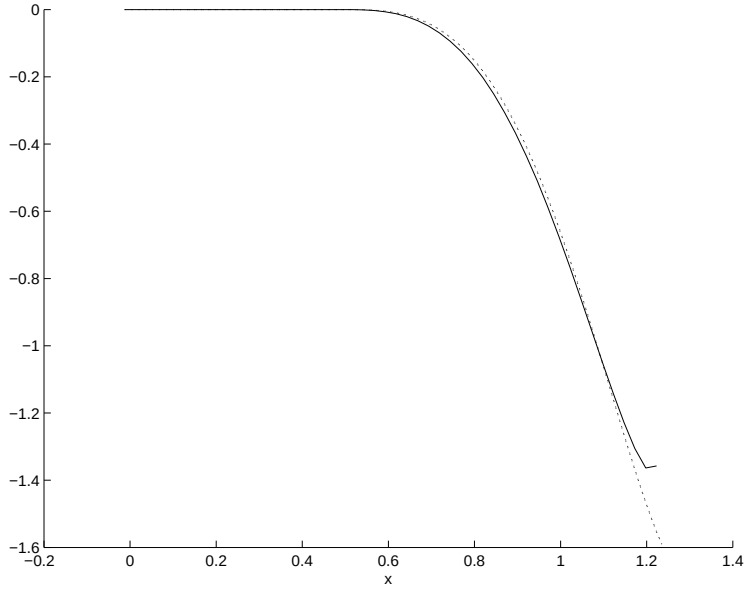

Figure 11: Order 1 scheme with shifted grid

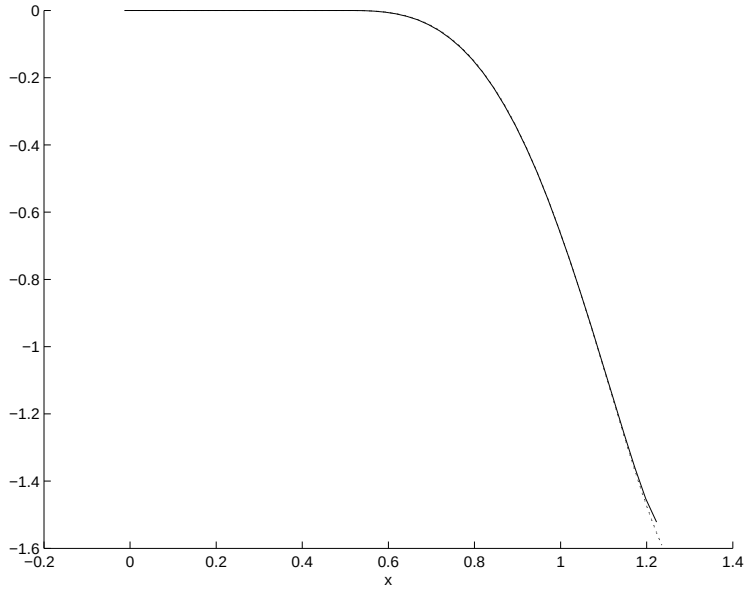

Figure 12: Order 2 scheme with shifted grid

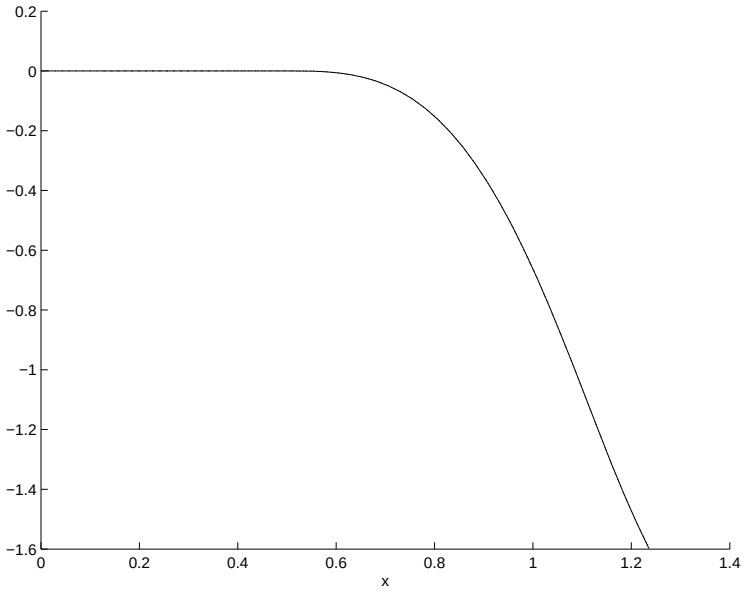

Figure 13: Our scheme

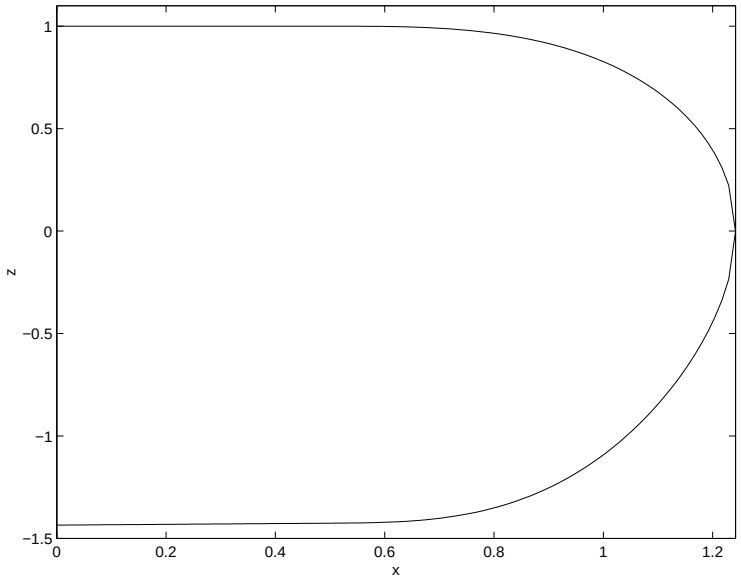

Figure 14: Graphs of Θ^- and Θ^+, z fixed

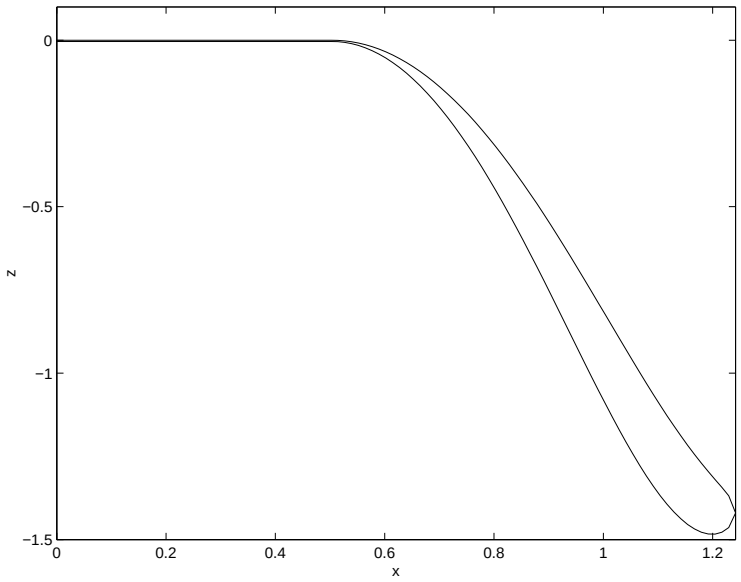

Figure 15: Graphs of Λ^- and Λ^+, z fixed

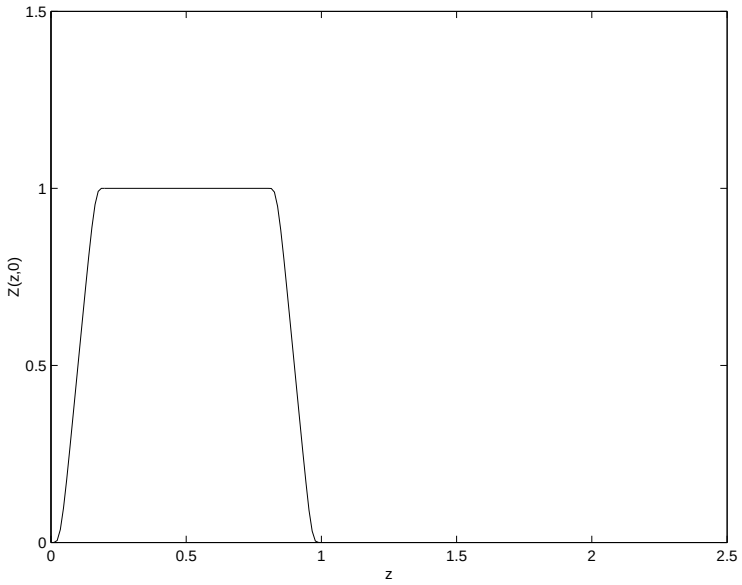

Figure 16: Incoming Z on the z axis

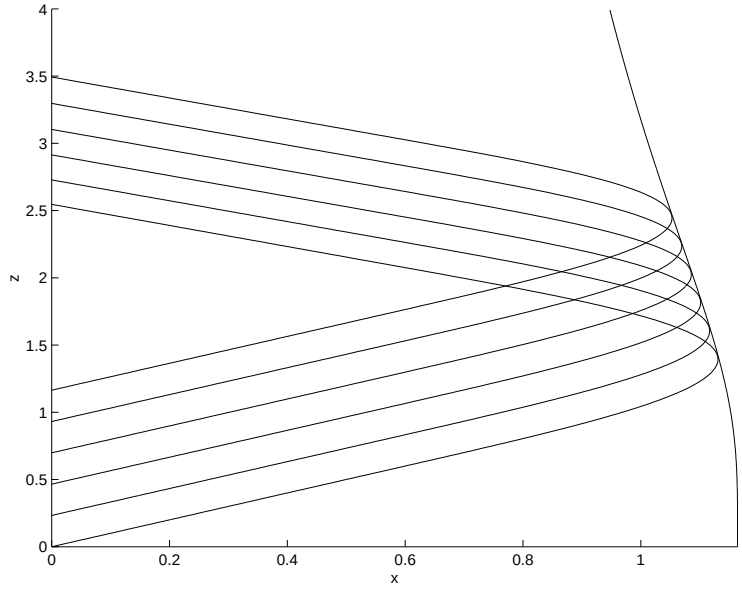

Figure 17: Comparison with the ray method

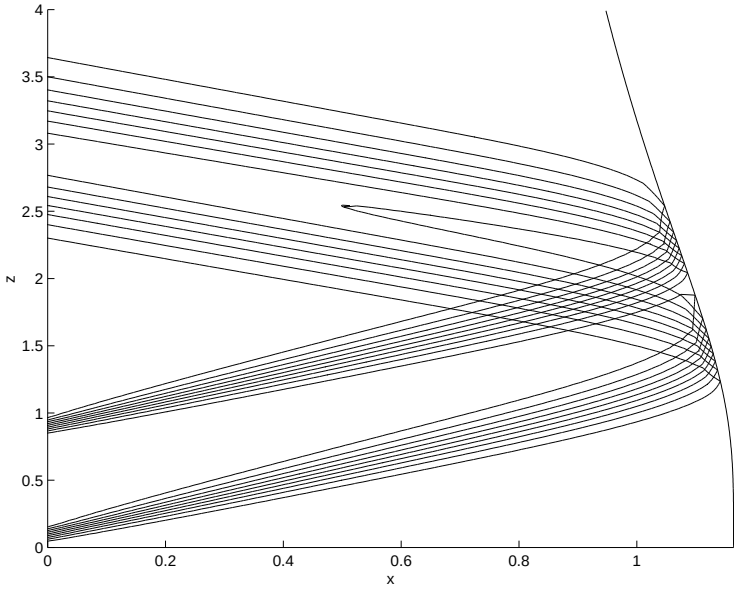

Figure 18: Contour lines of Z^- and Z^+

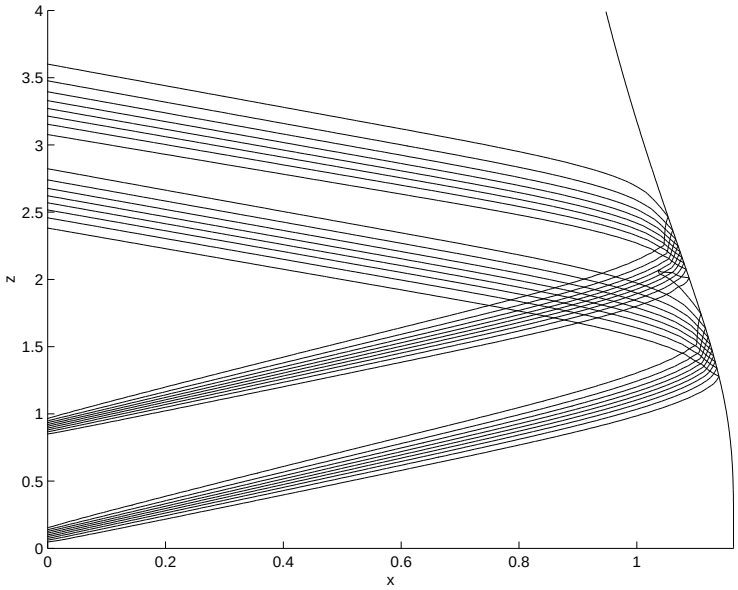

Figure 19: Contour lines of Z^- and Z^+ – Van Leer scheme

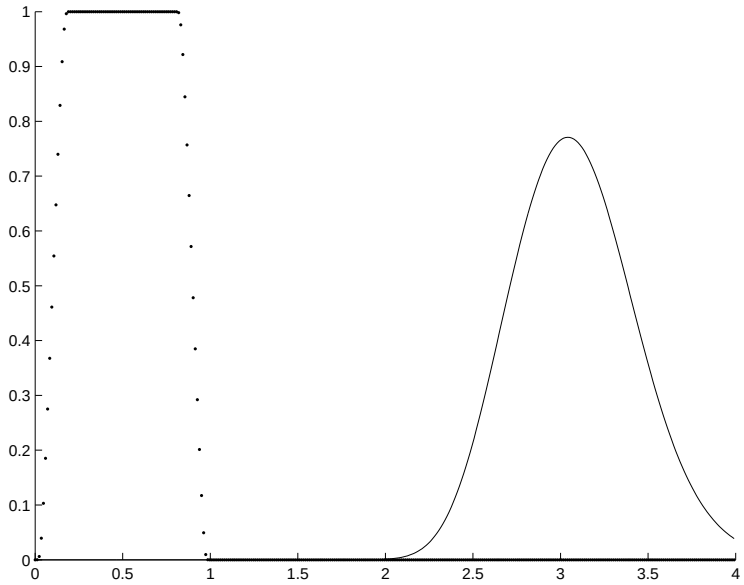

Figure 20: Z^- and Z^+ on $x = 0$

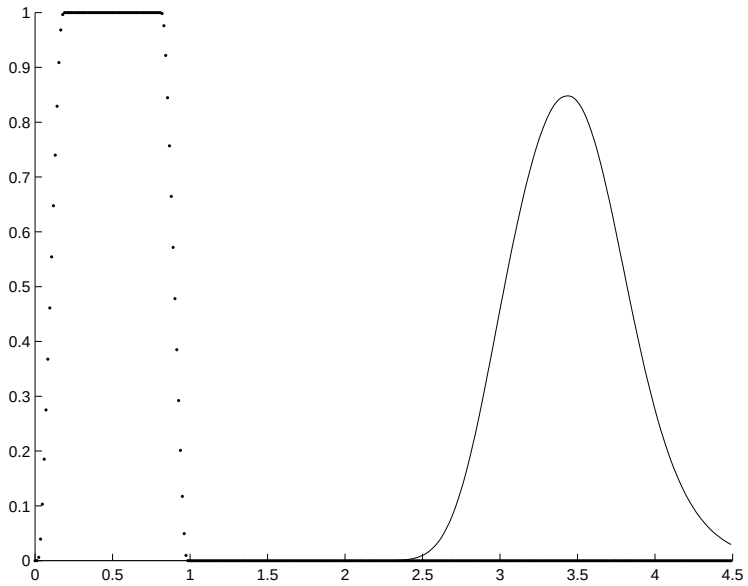

Figure 21: Z^- and Z^+ on $x = 0$ – Van Leer scheme, 50 points

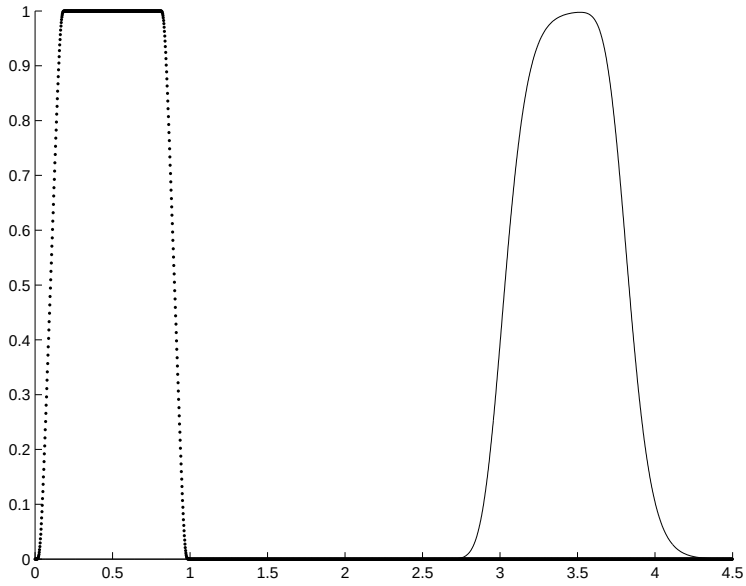

Figure 22: Z^- and Z^+ on $x = 0$ – Van Leer scheme, 300 points

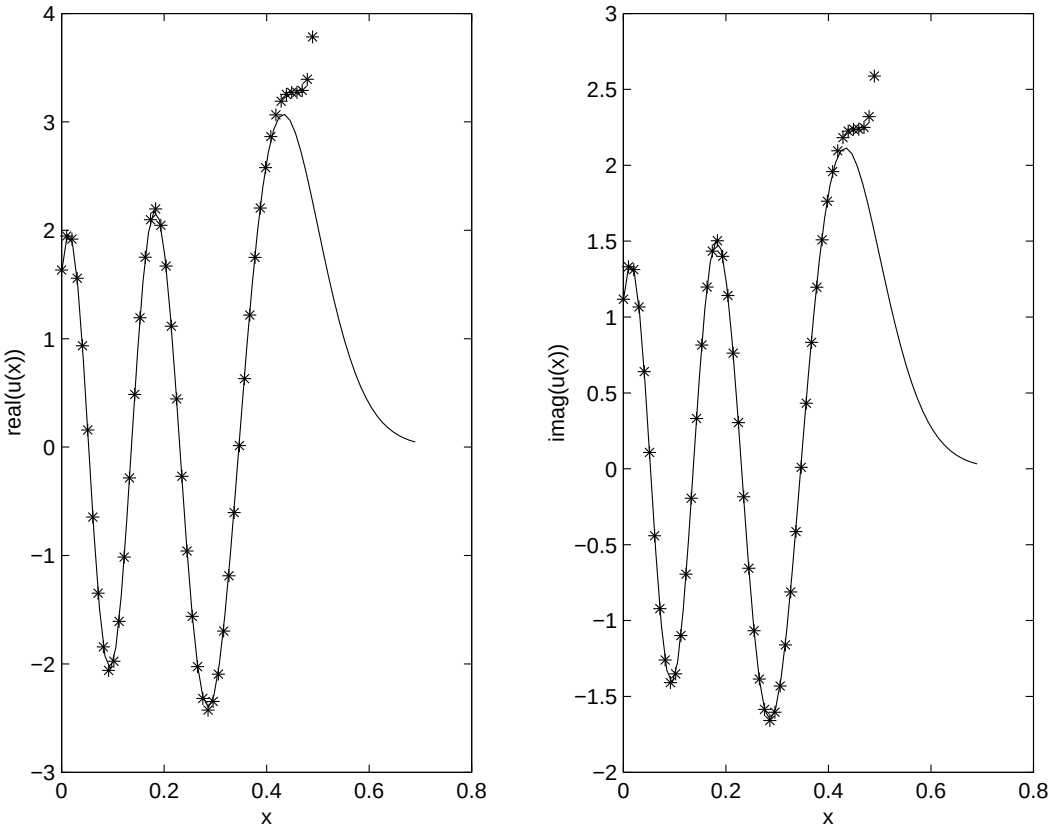

Figure 23: Pointwise comparison in the (43) case – $k_0 = 60$

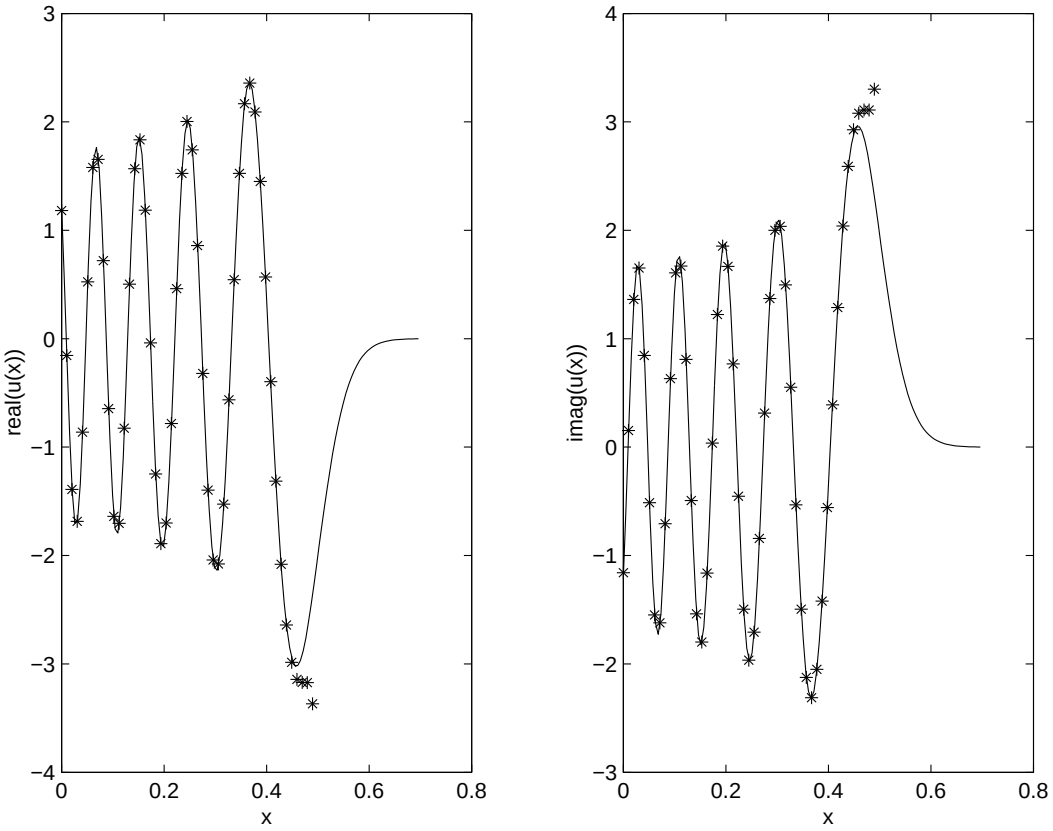

Figure 24: Pointwise comparison in the (43) case – $k_0 = 120$

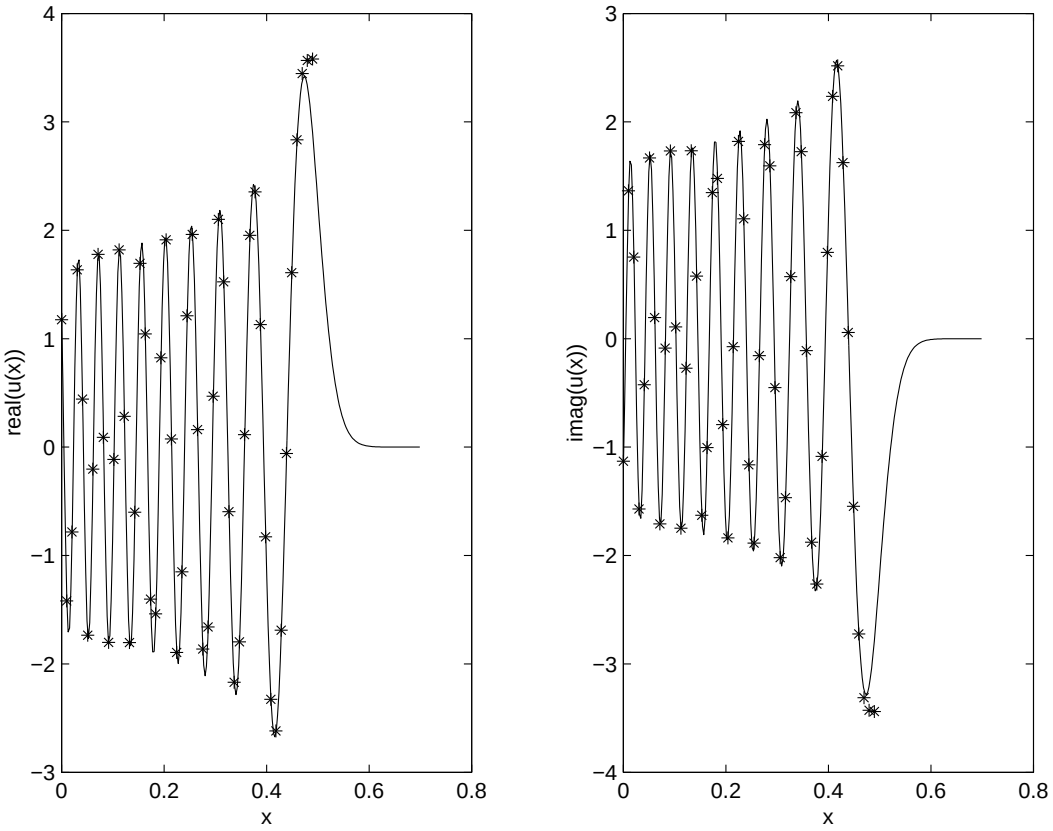

Figure 25: Pointwise comparison in the (43) case – $k_0 = 240$

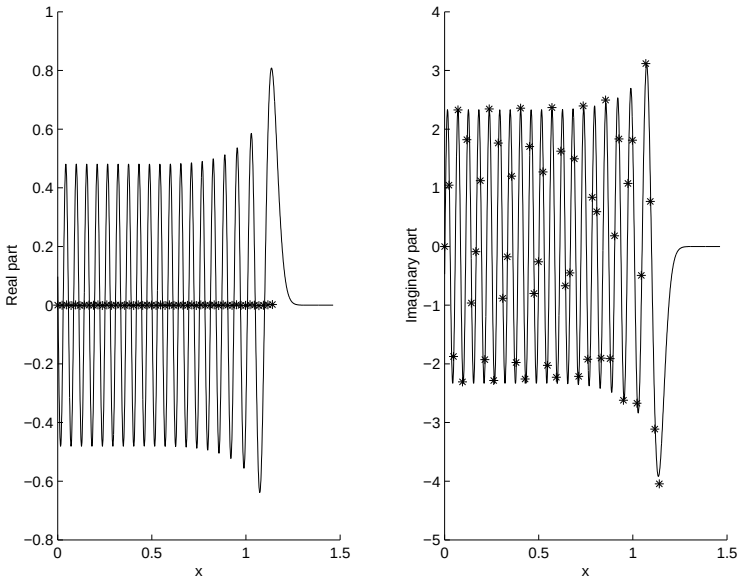

Figure 26: Pointwise comparison in the (44) case – $k_0 = 160$

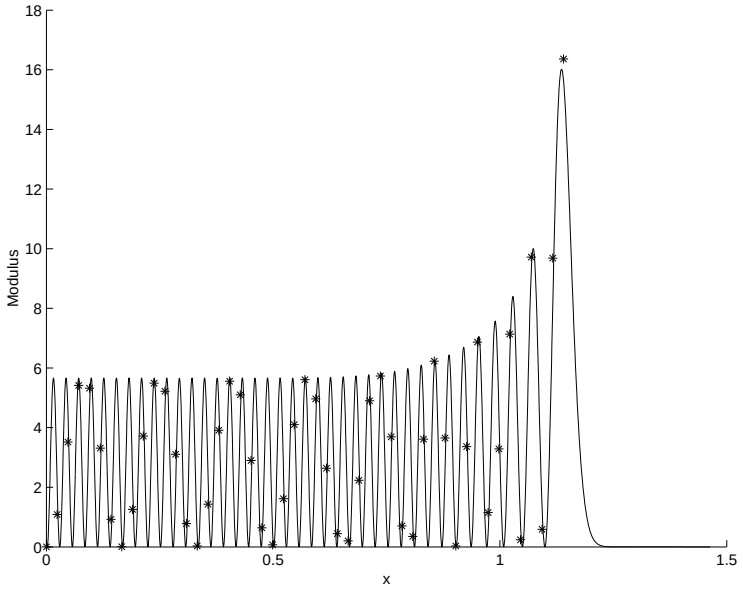

Figure 27: Pointwise modulus comparison in the (44) case – $k_0 = 160$

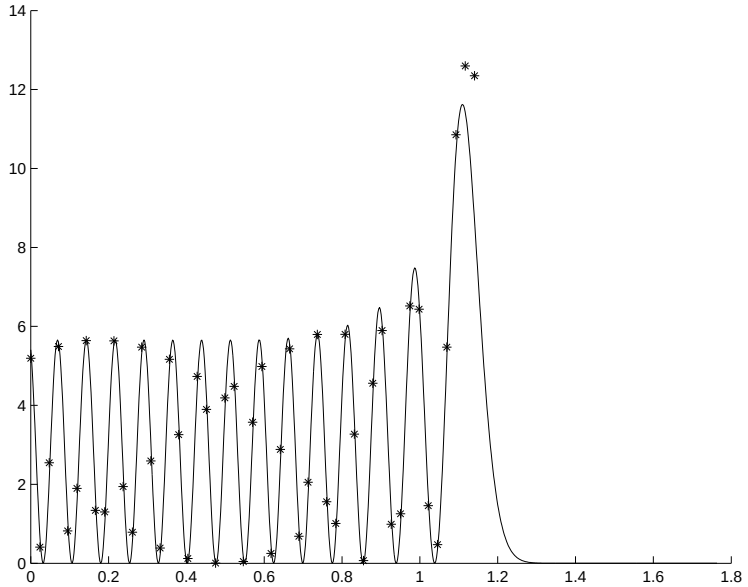

Figure 28: Pointwise modulus comparison in the (44) case – $k_0 = 60$

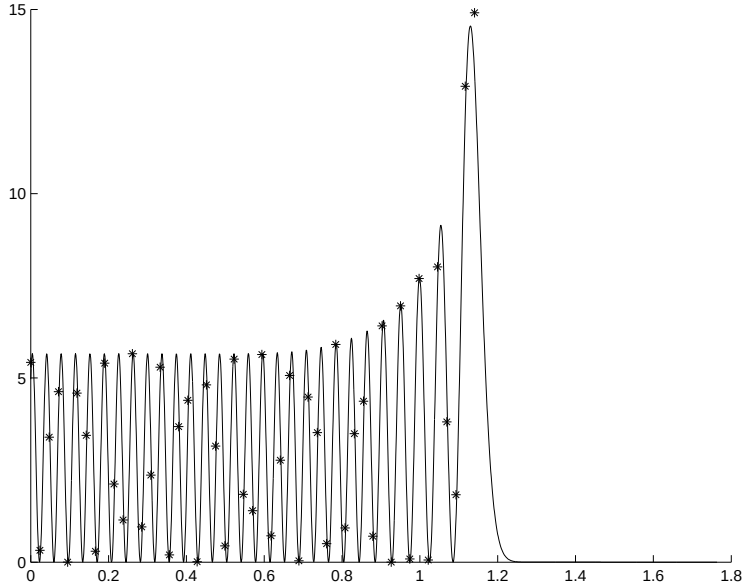

Figure 29: Pointwise modulus comparison in the (44) case – $k_0 = 120$

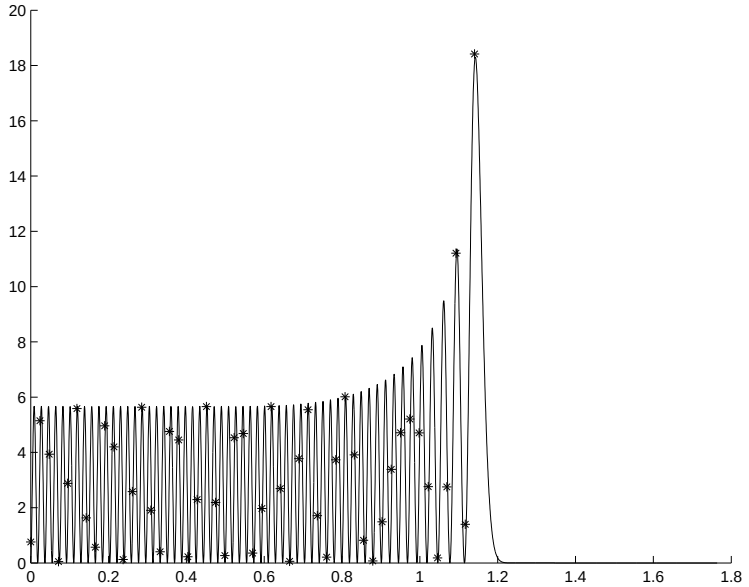

Figure 30: Pointwise modulus comparison in the (44) case – $k_0 = 240$

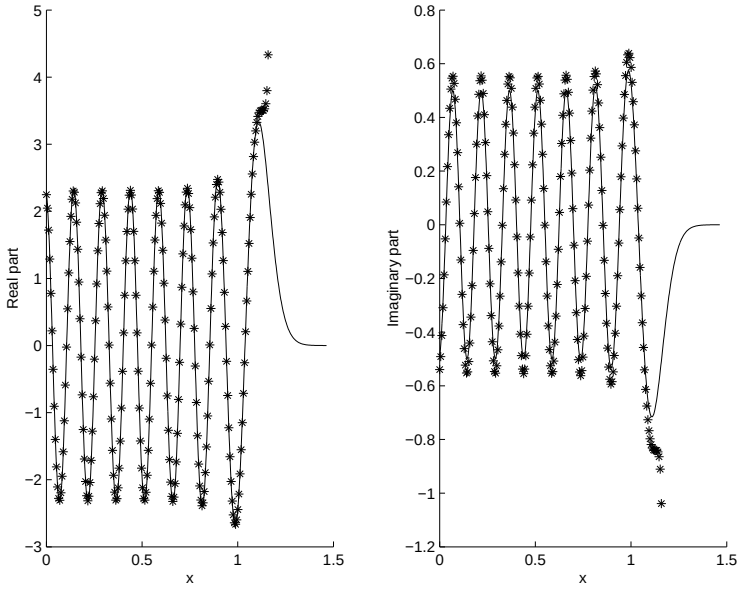

Figure 31: Pointwise comparison in the (44) case – $k_0 = 60$

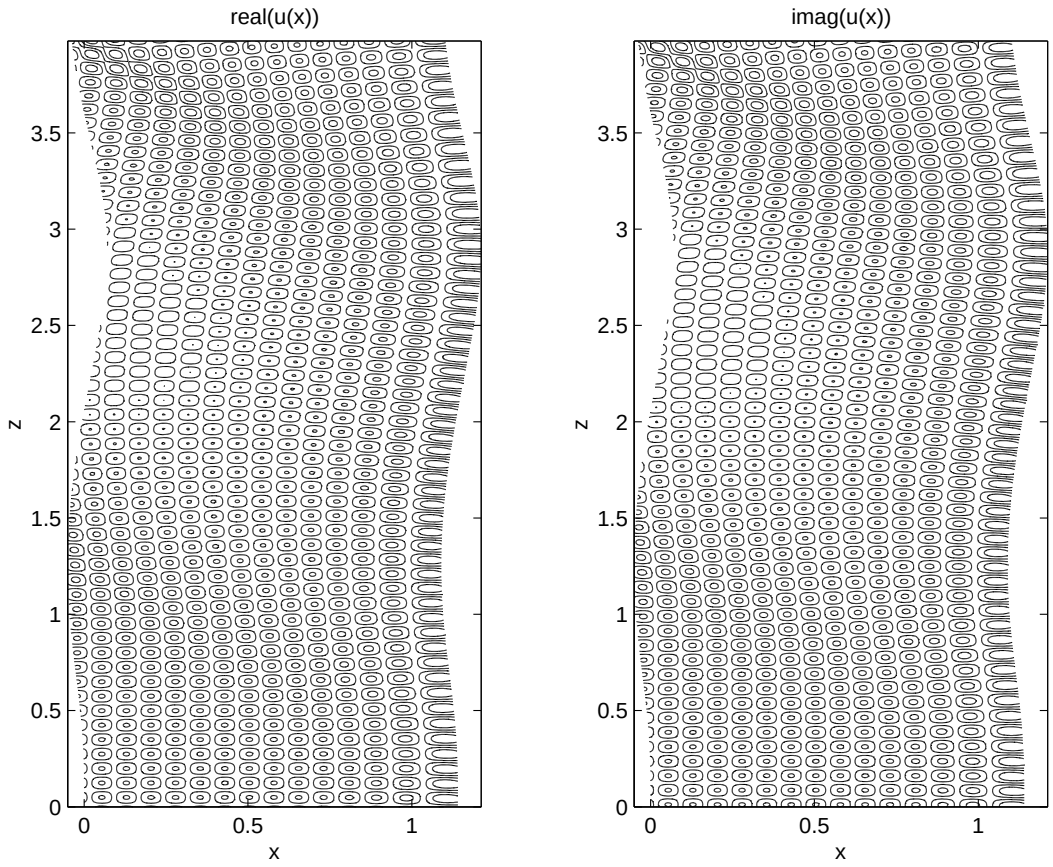

Figure 32: The (10) ansatz

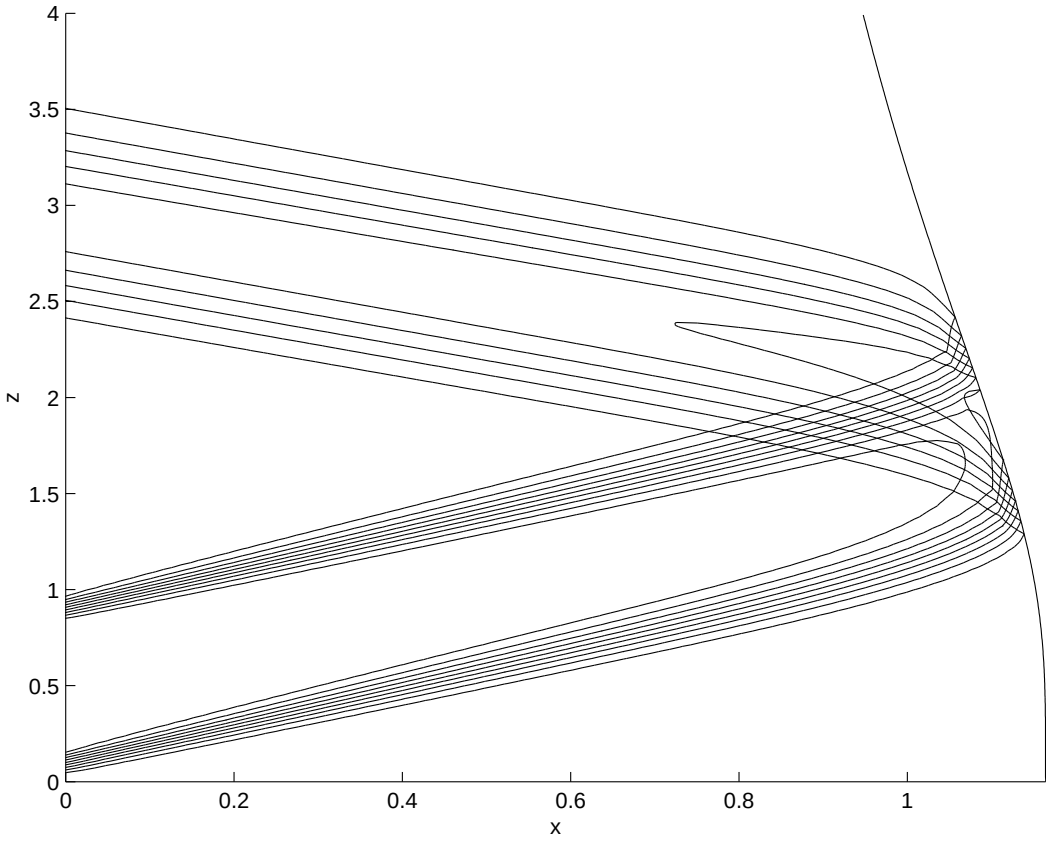

Figure 33: The contour lines of $Z^{\pm}$ with absorption

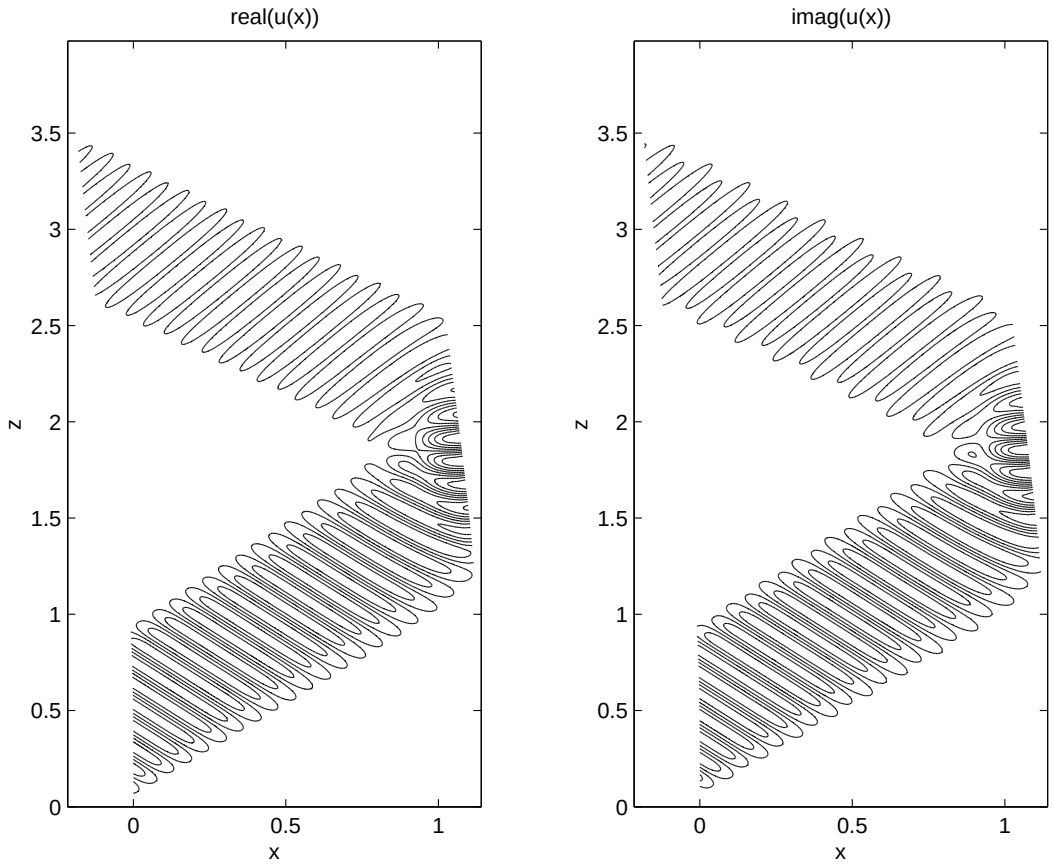

Figure 34: The (10) ansatz with absorption

Unité de recherche INRIA Rocquencourt
Domaine de Voluceau - Rocquencourt - BP 105 - 78153 Le Chesnay Cedex (France)

Unité de recherche INRIA Lorraine : LORIA, Technopôle de Nancy-Brabois - Campus scientifique
615, rue du Jardin Botanique - BP 101 - 54602 Villers-lès-Nancy Cedex (France)
Unité de recherche INRIA Rennes : IRISA, Campus universitaire de Beaulieu - 35042 Rennes Cedex (France)
Unité de recherche INRIA Rhône-Alpes : 655, avenue de l'Europe - 38330 Montbonnot-St-Martin (France)
Unité de recherche INRIA Sophia Antipolis : 2004, route des Lucioles - BP 93 - 06902 Sophia Antipolis Cedex (France)

Éditeur
INRIA - Domaine de Voluceau - Rocquencourt, BP 105 - 78153 Le Chesnay Cedex (France)
http://www.inria.fr
ISSN 0249-6399